International Journal of Innovations in Science & Technology

Volume 3
Issue 2

IJIST
P ISSN : 2618-1630
E ISSN : 2909-6130

Journal.50sea.com

50SEA

Prof Dr. Ali Iqtadar Mirza
Chief Editor
International Journal of Innovations in Science and Technology

Abstracting and Indexing

IJIST
P ISSN : 2618-1630
E ISSN : 2909-6130
Recognized Journal

Scientific Journal Impact Factor
TOGETHER WE REACH THE GOAL

Scilit

CiteFactor
Academic Scientific Journals

IOI JOURNALS MASTER LIST

IDEAS

INFOBASE INDEX

IPIndexing
Indexing Portal

RESEARCHBIB
ACADEMIC RESOURCE INDEX

ROOTINDEXING
JOURNAL ABSTRACTING AND INDEXING SERVICE

SIS

WIKIDATA

Instructions for Authors

The editorial board encourages and welcome true researches, laboratory experiments and real time field observations to get published in IJIST. The authors are advised to prepare their manuscript according to the template of IJIST.

Please see the checklist before submitting your manuscript to IJIST.

- The manuscript is prepared according to the template of IJIST.
- Symbols and names are used according to international standards.
- Page no and Line no are adjusted on the manuscript.
- Figure and Table are clearly cited.
- Author names and their affiliation are typed clearly.
- There is no any limit to the length of manuscript.
- Abstract is comprised of 250 words.
- Author's contribution and the statement narrating no of conflict of interest is mentioned in the end.
- Each Figure and Table is numbered and cited in the text.
- Spelling and English grammar is checked.
- It is "Open Access" journal that publish articles on payment of publishing fee by authors or by their institutions.
- All the articles are published under Creative Common License CC-BY therefore, authors mush agree with same license.

Aims and Scopes

The authors are advised to submit their manuscript in accordance with disciplines as below:

- Administrative Science
- Agriculture/Forestry
- Climatology
- Criminology
- Development Study
- Environment
- GIS
- Geography
- Meteorology
- Physics
- Remote Sensing
- Social Science
- Urban Planning
- Economics
- Chemistry
- Bio-Chemistry
- Computer Science

Peer Review Process

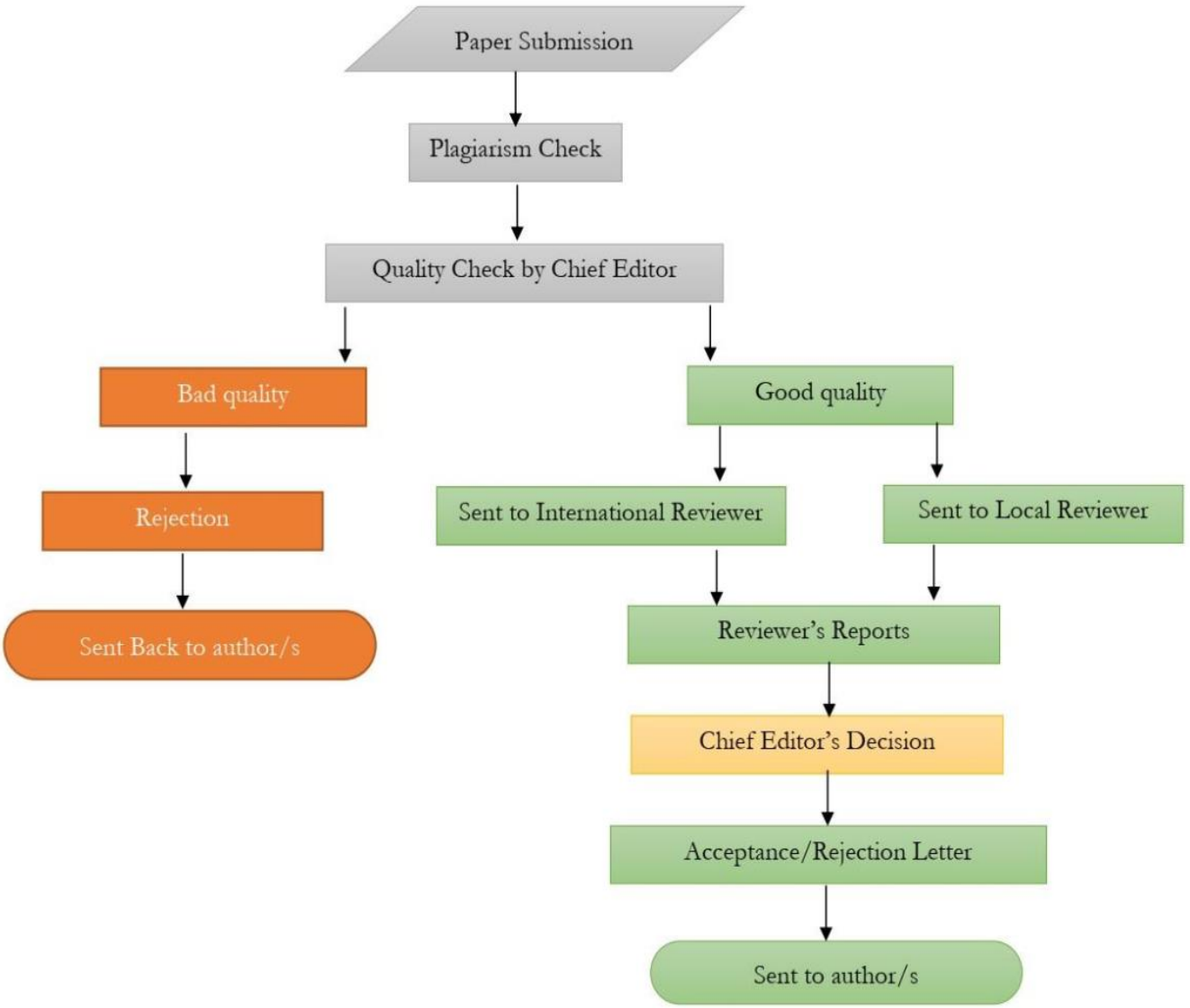

Table of Contents

International Journal of Innovations in Science & Technology (IJIST)

ISSN 2618-1630

V3-I2 | June 2021

IJIST
P ISSN : 2618-1630
E ISSN : 2909-6130

Temporal Variations in Ice Cap of Antarctica and Greenland

Abdul Baqi[1], Ali Abbas[2]
[1]Goverment Degree College Usta Muhammad, District Jaffarabad, Balochistan, Pakistan.
[2] Department of Geography, University of the Punjab
Correspondence: Abdul Bai, Baqiabdul123@gmail.com
Citation |Baqi.A, Abbas. A "*Temporal Variations in Ice Cap of Antarctica and Greenland*". International Journal of Innovations in Science & Technology, Vol 03 Issue 02: pp 52-58, 2021.
Received |March 19, 2021; Revised | March April 04, 2021; Accepted | April 08, 2021; Published | April 10, 2021.

Abstract.

The Antarctic and Greenland polar ice caps are the largest mass of ice in world. Globally the climate system is considerably affected by these ice sheets. Several natural and anthropogenic activities have affected the balance of mass of ice sheets. Ice sheets mass loss is a consequence of changes of patterns of precipitation, changing wind patterns, increasing global temperature and increased glacial flow. Nearly 75% of the ice mass loss has been observed in these regions since last ten years. A sharp increase in ice mass loss in Antarctic and Greenland regions are detected through 0.3mm increase in sea level per year. In this research paper Satellite remote sensing techniques including Enhanced Thematic Mapper Plus (ETM+) is used to monitor and reveal the patterns of ice melt and glacier flow in these regions.

Keywords: Antarctic ice sheet; Greenland ice sheet; snowmelt; dynamic monitoring; characteristics

Introduction

The global climate system is considerably affected by the world's largest ice sheets, the Antarctic and Greenland ice caps. The climate changes over a fraction of Antarctic and Greenland ice sheets has caused variations in snow water content which changes the reflectivity of surface of ice sheets, which disrupts balance of ice sheets in polar regions. Thus, the snowmelt in Polar Regions is of great significance for understanding the variations in global climate [1].

Antarctic and Greenland ice sheets have started losing mass since 1990 consequently raising the sea level. The loss of mass in Antarctic region has been increased thrice while the mass loss has been increased twice in Greenland from the years 2007 to 2016 [2]. One third of the total sea level has been raised since 1990 due to melting of polar ice caps [3].

Snow melts in Antarctic and Greenland ice caps are sensitive climate change indicators as these regions contain two third of the worlds fresh water in the form of ice sheets. Melting of these ice sheets will raise the level of water triggering the coastal

resettlements globally. Since 1990s sea level has been raised up to 7.4mm globally as a consequence of snowmelt [4].

The ultimate dynamics of snowmelts can be measured, monitored and assessed using satellite based observations. The ice melt surfaces reflect microwave radiations which can be effectively transmitted through clouds, thus snowmelt data can be effectively detected by satellites even in the presence of clouds. Variations in snowmelt, ice mass, snowfall, glacier flow and snow density is effectively detected by microwave brightness temperature (MBT) [5,6].

Thus space borne satellites can be used to monitor ice cap changes utilizing microwave brightness temperature. Satellite capabilities to monitor physical features and assessment of variations over these features have been enhanced since last 2 decades. Remotely sensed satellite imagery is being accurately used these days in order to obtain spatio- temporal data and assessment of variance in physical attributes of Earth [7,8,9].

Material and Methods

Study Area

The area under study includes Antarctic and Greenland ice sheets. Antarctica is the largest ice mass covering 98% of the Antarctic continent. It covers 5.4 million square miles area of world while Greenland ice sheet covers 1710000km^2 area of world and almost 79% region of Greenland.

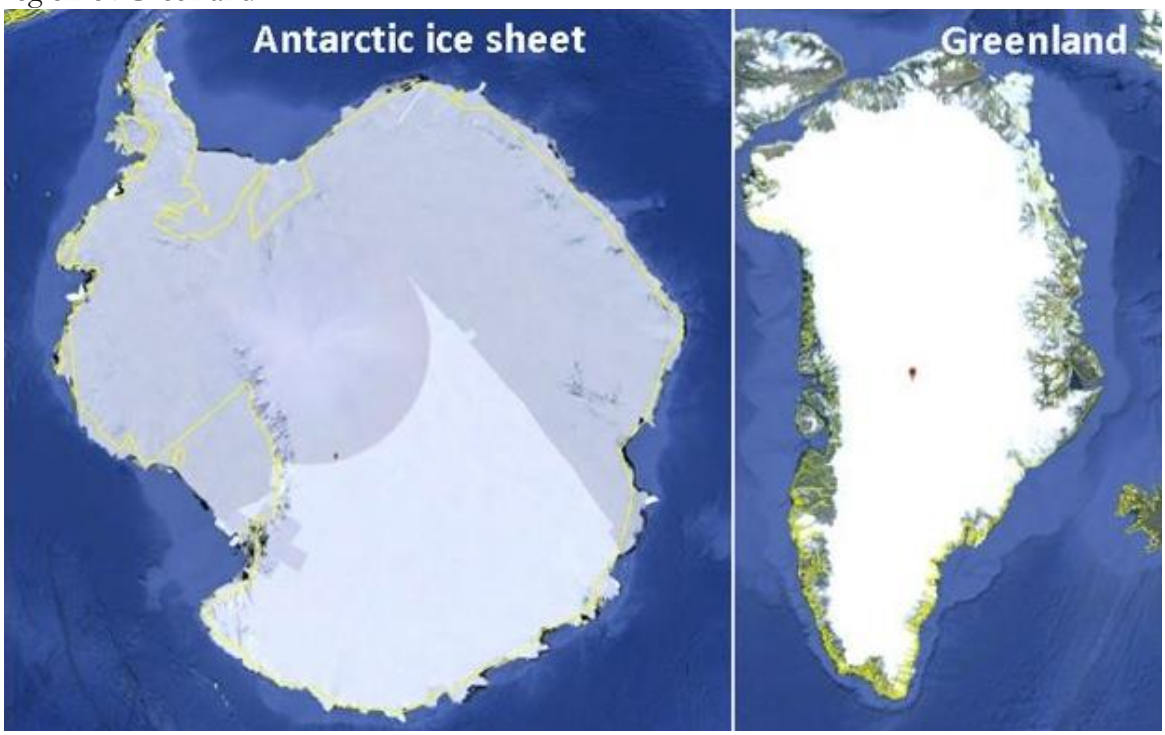

Figure 1. Antarctic and Greenland ice sheets.

Data Used

The datasets used in this research paper are obtained through spatio temporal satellite imagery and Atmospheric Infrared Sounder (AIRS) technology. The datasets were developed using microwave brightness temperature to monitor changes in ice cap [10,11].

Satellite imagery

The satellite images are obtained through Sentinel (https://sentinel.esa.int/) and Landsat (https://landsat.usgs.gov/) platform and from different sensors for instance Enhanced Thematic Mapper Plus (ETM+), including Thematic Mapper (TM), and Multi Spectral Instrument (MSI) [12,13,14].

Optical images

ENVI software was used to preprocess the acquired optical images. The images were first geo refrenced with the help JICA topographic data and GPS field surveys in accordance with the World Geodetic System the UTM projection [15]. Subsequently the images were processed for radiometric and geometric correction and then for re sampling. The atmospheric effects were reduced using radiometric correction, while the geometric correction removed the geometric distortion [17].

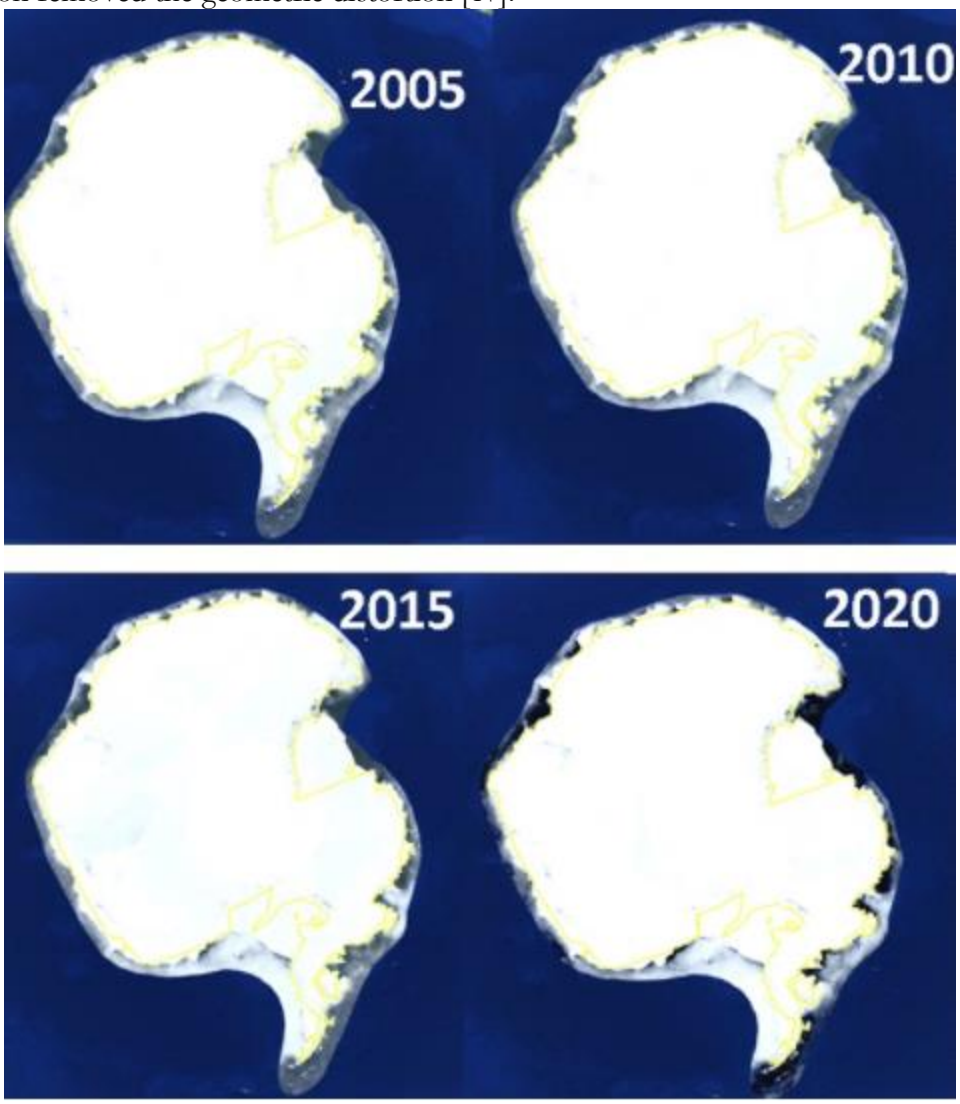

Figure 2. Ice sheets of Antarctica for the years 2005, 2010, 2015 and 2020.

Figure 2 shows the satellite imagery of the Antarctic continent for the years 2005, 2010, 2015 and 2020. The ice mass loss since 2005 to 2020 can be observed.

Results and discussion

The climate changes over a fraction of Antarctic and Greenland ice sheets has caused variations in snow water content which changes the reflectivity of surface of ice sheets, which disrupts balance of ice sheets in polar regions. The loss of mass in Antarctic region has been increased thrice while the mass loss has been increased twice in Greenland from the years 2007 to 2016. One third of the total sea level has been raised since 1990 due to melting of polar ice caps. Since 1990s sea level has been raised up to 7.4mm globally as a consequence of snowmelt.

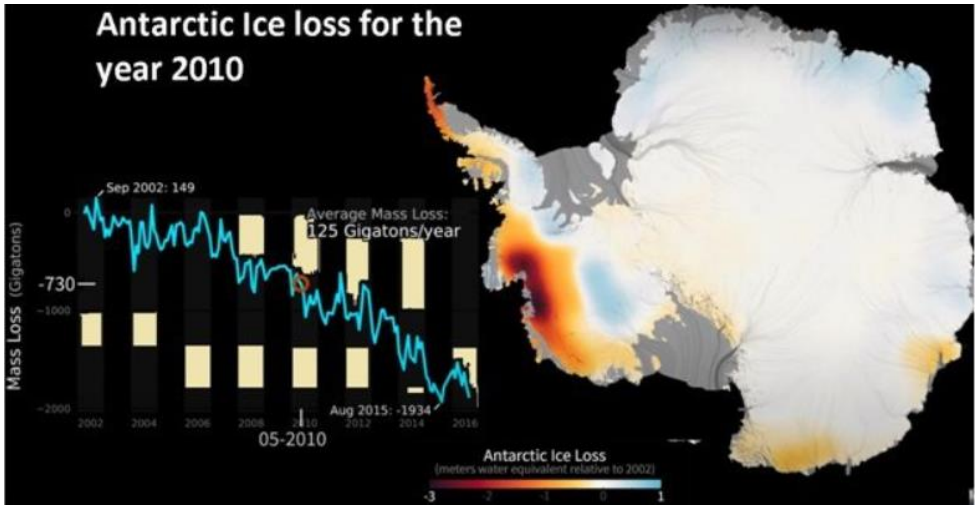

Figure 3. Graphical representation of ice mass loss for the year 2010 in Antarctica.

The figure 3 shows that the in the year 2010 Antarctic region lost up to -730 gigatons of ice mass. The average mass loss reached to 125 gigatons per year. According to NASA the net loss of ice mass in Antarctica increased from 112 to 196 gigatons from the year 1996 to 2006. The sea level rises up to 0.35 mm per year due to this ice mass loss.

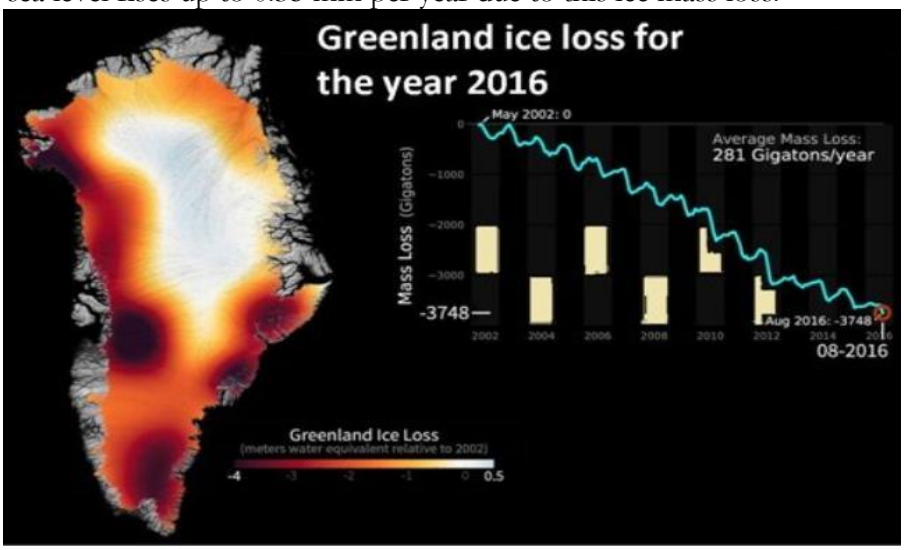

Figure 4. Graphical representation of ice mass loss in the Greenland for the year 2016.

Figure 4 shows mass loss in Greenland was up to -3748gigtons by the year 2016. The average rate of ice loss in Greenland is 281 gigatons per year. According to NASA sea level raises up to 0.03 inches per year due to this ice loss. The Greenland ice sheets were gaining ice mass until 1970s, but the ice mass became decreasing since 1980s by increasing global temperature. Since 19th centaury the average 1.2°C temperature rise has affected the ice sheets in Polar Regions. Temperature rise triggered melting of snow, development of glacial lakes, changed wind and tidal patterns and raised water level of sea. The total Antarctic snow melt extent decreased by 2488.44 ± 7131.63 km2/year, and the snowmelt index decreased by 279900.54 ± 238729.96 day*km2/year from the year 1978 to 2014 while the snow melt extent of the Greenland ice sheet is less than that of Antarctica, and the average area affected was 764,000 km2 for 1978–2014.

Conclusion

In this research paper Antarctica and Greenland ice sheets have been analyzed using remotely sensed satellite data to monitor the loss of ice mass since 1990s. The results showed that these regions were gaining ice mass till 1970 later on the ice mass was lost due to increasing global temperature. Average 1.2°C rise in temperature has triggered climatic changes globally. According to NASA the net loss of ice mass in Antarctica increased from 112 to 196 gigatons from the year 1996 to 2006 while the average rate of ice loss in Greenland is 281 gigatons per year.

Conflicts of Interest

The authors declare no conflicts of interest regarding the publication of this paper.

References

1. Meier, F. Ice, Climate and sea level. Do we know what is happening? In Ice in The Climate System; Peltier, W.R., Ed.; Springer Link: Berlin/Heidelberg, Germany, pp. 141–160, 1993.
2. Liu, H.; Wang, ; Jezek, K. Wavelet-transform based edge detection approach to derivation of snowmelt onset, end and duration from satellite passive microwave measurements. Int. J. Remote Sens. Vol 26, pp: 4639–4660, 2005.
3. Haggerty, A.; Curry, J.A. Variability of sea ice emissivity estimated from airborne passive microwave measurements during FIRE SHEBA. J. Geophys. Res. Atmos. Vol 106, pp; 15265–15277, 2001.
4. Lee, S.-M.; Sohn, B.-J. Retrieving the refractive index, emissivity, and surface temperature of polar sea ice from 6.9 GHz microwave measurements: A theoretical development. J. Geophys. Res. Atmos. Vol 120, pp: 2293–2305, 2015.
5. Skofronick-Jackson, M.; Gasiewski, A.J.; Wang, J.R. Influence of microphysical cloud parameterizations on microwave brightness temperatures. IEEE Trans. Geosci. Remote Sens. Vol 40, pp: 187–196, 2002.
6. Zwally, J.; Gloersen, P. Passive microwave images of polar regions and research applications. Polar Rec. Vol 18, pp: 431–450, 1977.
7. Ulaby, T.; Moore, R.K.; Fung, A. Microwave Remote Sensing: Active and Passive; From theory to application; Artech House: Norwood, MA, USA, Vol 3, 1986.
8. Mote, L.; Anderson, M.R.; Kuivenen, K.C.; Rowe, C.M. Passive microwave-derived spatial and temporal variations of summer melt on Greenland ice sheet. Ann. Glaciol. Vol 17, pp: 233–238, 1993.

9. Zwally, J.; Fiegles, S. Extent and duration of Antarctic surface melting. J. Glaciol. Vol 40, pp: 463–476, 1994.
10. Steffen, ; Abdalati, W.; Stroeve, J. Climate sensitivity studies of the Greenland ice sheet using satellite AVHRR, SMMR, SSM/I and in situ data. Meteorol. Atmos. Phys. Vol 51, pp: 239–258, 1993.
11. Abdalati, ; Steffen, K. Greenland Ice Sheet melt extent: 1979–1999. J. Geophys. Res. Vol 106, pp; 33983–33988, 2001.
12. Takala, ; Pulliainen, J.; Huttunen, M.; Hallikainen, M. Estimation of the beginning of snow melt period using SSM/I data. In Proceedings of the IEEE International Geoscience and Remote Sensing Symposium 2003 (IGARSS), Toulouse, France, 21–25 July 2003.
13. Joshi, ; Merry, C.J.; Jezek, K.C.; Bolzan, J.F. An edge detection technique to estimate melt duration, season and melt extent on the Greenland ice sheet using passive microwave data. Geophys. Res. Lett. Vol 28, pp; 3497–3500, 2001.
14. Liu, H.; Wang, ; Jezek, K. Spatio-temporal variations of snow melt zones in Antarctic Ice Sheet derived from satellite SMMR and SSM/I data (1978-2004). J. Geophys. Res. , Vol 111, 2006.
15. Aschraft, S.; Long, D.G. Comparison of methods for melt detection over Greenland using active and passive microwave measurements. Int. J. Remote Sens. Vol 27, pp: 2469–2488, 2007.
16. Torinesi, ; Fily, M.; Genthon, C. Variability and trends of the summer melt period of Antarctic Ice margins since 1980 from Microwave sensors. J. Clim. Vol 16, pp: 1047–1060, 2003.
17. Tedesco, Assessment and development of snowmelt retrieval algorithms over Antarctica from K-band spaceborne brightness temperature (1979–2008). Remote Sens. Environ. Vol 113, pp: 979–997, 2009.

OPEN ACCESS International Journal of Innovations in Science & Technology

IJIST
P ISSN : 2618-1630
E ISSN : 2909-6130

Monitoring of Mangrove Cover of Western Indus Delta Karachi Pakistan

Nasir Abbas[1], Nimra[1], Warda Habib[1]
[1]Department of Geography Government College University Lahore, Pakistan
* Correspondence: Nasir Abbas (nasirgcu@gmail.com)
Citation | Abbas. N, Nimra, Habib. W "Monitoring of Mangrove Cover of Western Indus Delta Karachi Pakistan". International Journal of Innovations in Science & Technology, Vol 03 Issue 02: pp 59-66, 2021.
Received |March 27, 2021; Revised | April 15, 2021; Accepted | April 20, 2021; Published | April 25, 2021.

Abstract
The coastline of Pakistan comprises of five significant sites comprising of mangroves including Indus Delta which contains extensive mangroves zones and termed as the largest arid mangrove found globally. This study evaluate the current extent of mangroves along the Western edge of Indus Delta and provide the most recent forest cover assessment of mangroves. Moreover, this study identifies the changes occurred in forest cover from the years 2000 to 2020. Landsat 5 Thematic Mapper (TM), 8 Operational Land Imager (OLI) and Landsat 7 ETM data were used for mangroves mapping through supervised classification method. The results displayed that total area of mangrove forest cover was nearly 279.094km², 395.77km², 306.58km² in the years 2000, 2010 and 2020 respectively. This study indicates an increase in area of mangrove cover from 29% to 41% from the year 2000 to 2010. Regeneration of mangrove mostly took place around the southern region of the Indus Delta. The mangrove specie has decreased from 41% to 31% from the year 2010 to 2020. The major causes of this reduction were urban water and industrial pollution, over-fishing in Indus delta, freshwater diversion for agriculture, and overharvesting of mangroves by the local communities, coastal erosion and sedimentation.
Keywords: mangrove; specie; arid; industrial pollution; Thematic Mapper.

Introduction

Mangroves forests are the valuable ecosystem for marine and coastal life, found in the intertidal zones of tropics and subtropical regions of world. These play a vital role as barriers between land and sea and act as natural shield against land erosion, tropical cyclones, and disasters and protect the shoreline [1]. Mangrove forests act as a shield for coastal areas to cope with flood, which are often affected by oceanic waves or rainstorms. Mangroves are the most diverse and productive ecosystems on planet earth. These forests have unique characteristics; which can survive under harsh saline environmental conditions [2]. The favorable environmental conditions for growth of mangroves forests are muddy soil, enough

rainfall and temperature ranging from 26-28ºC. Mangroves forests are beneficial for both human as well as natural environment [3]. The vegetated are useful habitats for estuarine species, fish, bivalves, crustaceans and birds providing them with food and protection. Nearly two million kilogram of the fish is produced with the support of mangroves and sea grass bed annually. Mangroves are also economically beneficial for local communities providing them with timber, fuel and fodder. Mangroves act as sink of carbon which grows in coastal areas to limit the outbreak of mosquitoes [4].

Mangrove forests are under the serious threat these days. During the last two decades of twentieth century, about 35% of the World mangrove forests disappeared. According to Splading 2006, the area under mangroves was estimated as 181000 km^2 globally during 1997 [5]. According to Giri 2014, this area reduced to 137760 km^2 in 2011 and then to 83495 km^2 stated by Hamilton and Casey in 2016. Anthropogenic activities including coastal urbanization, port development, conversion to agricultural land and over exploitation of timber and aquaculture played a vital role in this decline. Growth in aquaculture resulted with 38% of mangrove loss globally [6, 7, 8].

The coastal belt of Pakistan is extended up to 1050 km^2 in Sindh (350 km^2 and Baluchistan (700 km^2) [9]. About 97% of mangrove forests of Pakistan are located in the province of Sindh along the Indus Delta which cover about 600,000 ha, stretched from Korangi Creek in the north to Sir Creek in the south. Indus delta consists of 17 major creeks along various minor creeks and widespread mudflats [10].

The survival of mangrove vegetation requires a continuous supply of water from sea to survive in the deltaic region. The raising vegetation is irrigated by tidal water which in 24 hours runs twofold over the islands [11]. Avicenna is the chief cultivated crop in the area, which is determined by the range of tidal water. The crops grow faster closer to creek but growth descends rapidly inside the island. It is believed that the Indus delta had about eight mangrove species in past, out of which four still thrive. About 95% of the mangrove species found along the Indus delta which are Avicennia marina, Ceriop-stagalandAegicerascorniculatumare [12]. IUCN and WWF have been actively involved in Sindh and Balochistan for the active rehabilitation and conservation programs of mangrove. From 1985 IUCN Pakistan, in cooperation with the Sindh Forest Department, has jointly executed mangrove restoration programs along the coastline of Sindh [13, 14, 15]. These rehabilitation programs are executed along the coast by the involvement of local community. The main objective of this research was to monitor mangrove cover (in both degradation/upgradation) along the coastline.

Study Area

The study site included Western side of Indus Delta, Karachi. It is located on the bank of Arabian Sea; the Delta is circumvented by elongated and slim creeks, mud flats and by the Arabian Ocean mangroves of the Indus Delta, which is the biggest mangrove forest ecosystems found in parched climate [16]. Port Qasim is located on the fringe of river Indus at thirty-five kilometers east in Karachi. Port Qasim is located on the northwest fringe of the Indus Delta (Figure 1). It is the second busiest port of Pakistan, controlling thirty five percent of the country's shipment (seventeen million tons annually) [17,18]. About ninety percent of the external trade of the country is handled along with Port Qasim and Karachi Port. So, Indus delta is providing natural and economic benefits.

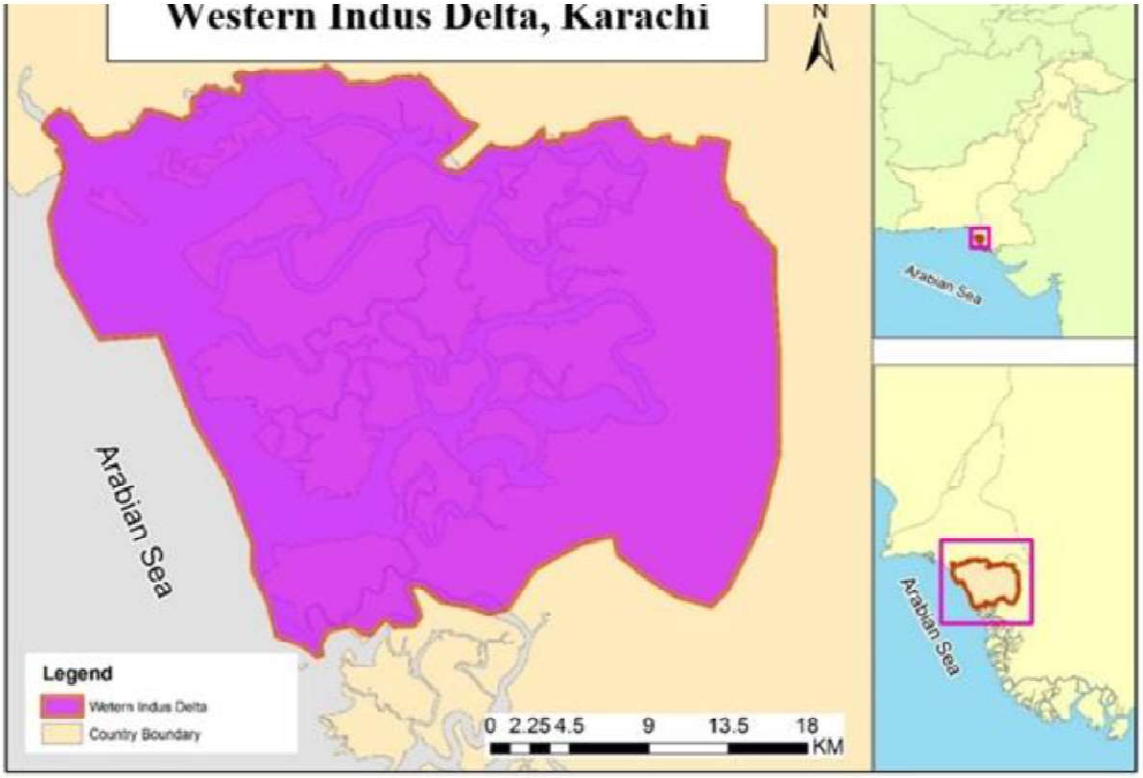

Figure 1. Study Area Map of Western Indus Delta, Karachi

Data and Method

Image Data

Digital satellite data is freely available and downloaded from USGS website for the years 2000, 2010 and 2019 and layer stacking of spectral bands was executed [19,20].

Table 1. Satellite data acquisition details

Image Acquisition Dates	Satellite	Resolution
28-01-2000	Landsat 5 thematic Mapper TM	30m
20-01-2010	Landsat & ETM	30m
22-01-2020	Landsat 8 operational land Imager (OLI)	30m

Supervised Classification (Maximum Likelihood)

After extraction of desired area, supervised classification (maximum likelihood) was performed in ARC GIS 10.3 to meet the requirements of research goals [21,22].With the help of classification tool bar Polygons were drawn for each sample object. The area was classified into major classes as Mangroves, Water, Mudflats and Sand.

Signature files were created of these sample objects [23]and maximum likelihood classification technique was applied. In input raster field, image layer was added and in input signature file the created signature file was added[24].

Results and Discussions

Current study evaluates the existing status and spatial distribution of Mangroves along the western part of Indus delta, Karachi. Land maps of study site were designed using pixel-based classification technique in ARC GIS 10.3 software.

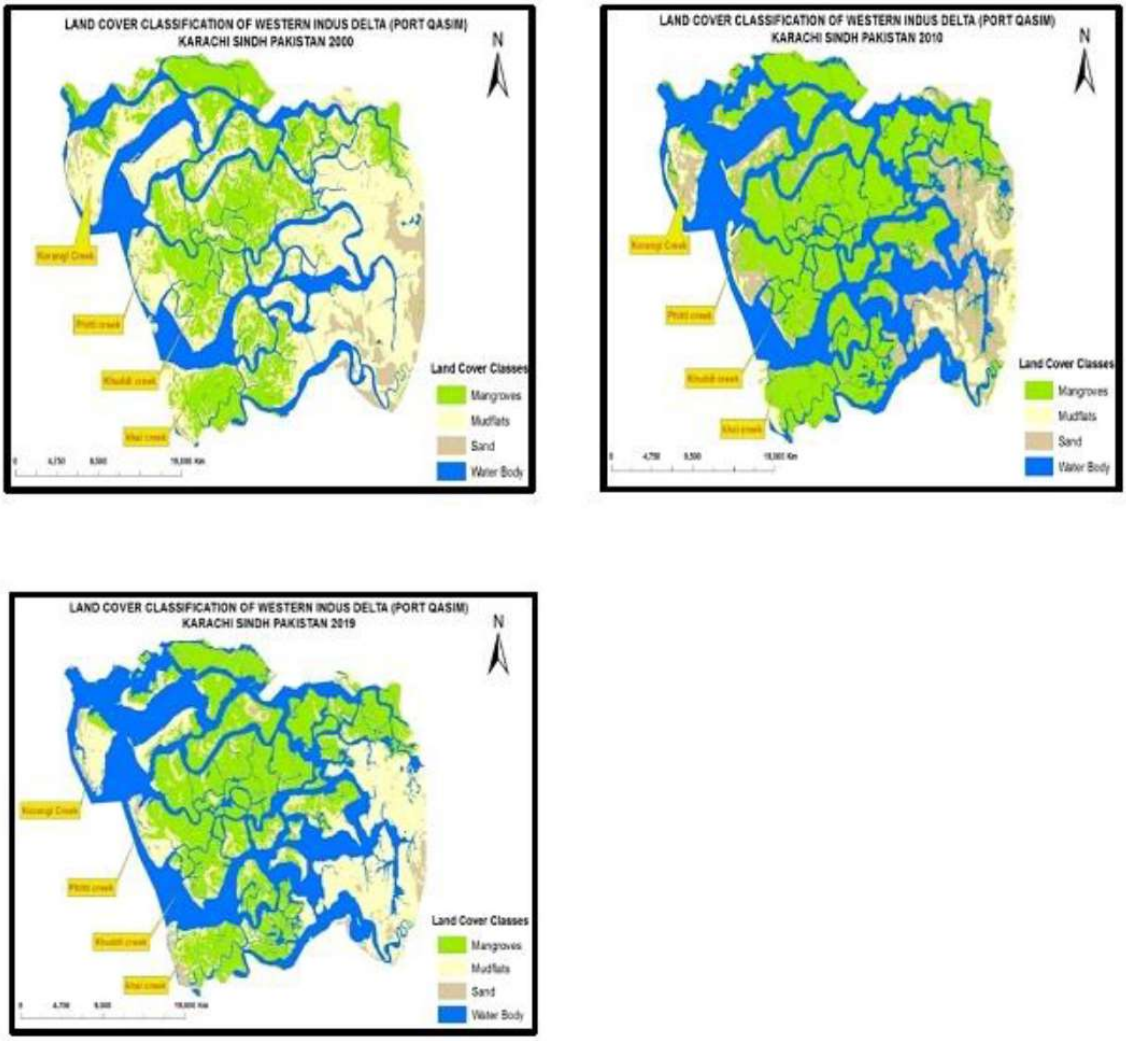

Figure 2. Land cover classification of western Indus delta of year (2000), (2010) and (2020)

Analysis of Land Cover Classes for the year (2000)

The land cover map of the year (2000) shows the clear distribution of four classes of land cover including mangroves, water body, mudflats and sand (Figure 2). The statistical data calculated by the pixel-based classification gives the accurate description of land cover. According to which, the mangroves occupy 279.0944km² which is about 29.10% of the total area. Water is about 215.22km² of the total area. Mudflats dominate with 405.183km² of the total area and sand covers about 59.36km².

Analysis of Land Cover Classes for the year (2010)

According to the pixel-based classification, mangroves covered 395.065km² area of study site which was about 41.27% of the total area. Water covered about 349.065km² of the total area

which was 36.40% of total area, Mudflats covered 71.966km² which was about 7% of total area and sand covered about 142.079km² of the total area.

Analysis of Land Cover Classes for the year (2020)

The statistical data calculated by the pixel-based classification for the year 2020 provides the accurate description of land cover. According to these statistics, the area covered by mangroves diminished up till 306.58km² of the total area which was about 31.97%. Water dominated with 374.43km² of the total area which was 39.04%, Mudflat occupied 251.76km² areas which was about 26.25% of total area and sand covered about 26.096km².

This study used maximum likelihood classification technique for different land cover classes. The varying trends in land cover from 2000 to 2020 have been observed (Figure 2). This study indicates overall 12.17% increase in mangrove area from 2000 to 2010 while reduction phenomenon was observed about 10.3% from 2010 to 2020.

In 2000, mangrove area was 29.1% of the total area covered area, which was further increased up to 41.27% in year 2010 of the total area and then again decreased up to 30.97% of total area. The results further reveal that, the percentages land covers of mudflats and water also varies from 2000 to 2020. For this variation visual comparison of resultant classified images have been applied which shows clear differences between land cover classes for respective years.

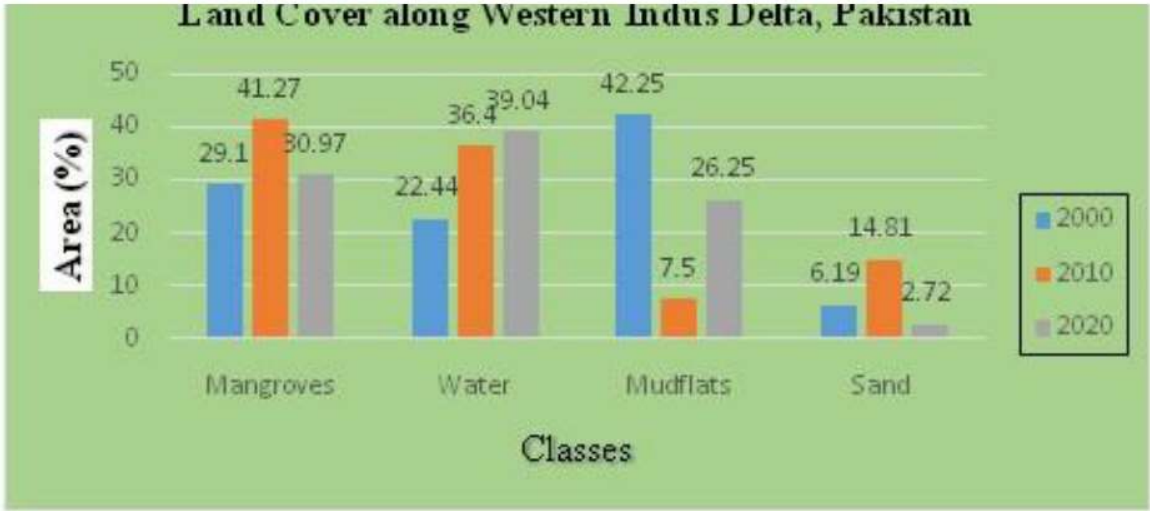

Figure 3. Bar graph of Land Cover Area Along Western Indus Delta

Comparison of Land Covers (2000-2010-2020)

The result of classified images showed that mudflats dominate the study area, approximately 42% of the total land is mudflats and 36% of the total area is water. The change detection illustrates the decrease in mudflats area and increase in water area from 2000 to 2020. The analysis of the year 2000 indicates that the total area of mangrove cover in the western side of Indus delta was about 279.0944km² ranging from Korangi creek to Khai Creek. In Landsat image of 2000, sand cover has also been classified with an area of about 59.36km². Other land cover statistics are given in Table 2. Landsat image of 2010 analysis show that the total cover of mangrove area was about 395.7759km² and sand was142.07km².

This approach represented an increasing trend in mangrove area from 2000 to 2010 and a decreasing trend from 2010 to 2020. The changes in the expansion of mangrove were observed in 2010. Figure 3 shows the bar graph of Land Cover area Along Western Indus

Delta. Most of expansion can be seen in southern part whereas in Northwest part of mangroves has not changed. The increase in mangroves vegetation in the above-mentioned year was because of natural regrowth along southern part. Human efforts were among contributing factors for the rehabilitation of mangrove plantation. But these days mangroves are under threat and continuously decreasing. The reasons behind this decrease are the climatic factors, anthropogenic activities, and the negligence of governmental institutions and over cutting of the specie by the local community. There is a need of replantation of the specie by the active participation of the locals and the governmental and non-governmental agencies for the rehabilitation of the mangroves. The huge area of mudflats can be used as potential rehabilitation sites therefore some vegetation efforts are observed in unfertile areas of mudflats.

Conclusion

Mangrove forests are most beneficial ecosystem of earth. It provides habitat and food to marine life, protects the shoreline from erosion and is home to many species. It provides social and economic benefits. In Pakistan mangrove forests are found in province of Sindh and Baluchistan. In Sindh 97% of the total mangrove are found along Indus River and in Baluchistan there is only 3%. In this study the land covered by mangrove forest is analyzed at Western Indus delta to access the change in mangroves covered area and to evaluate the causes of the degradation of specie. An increasing trend in mangroves vegetation has been observed from years 2000 to 2010. The vegetation increased up to 12% of the total area during these years and then a decreasing trend has been observed from years 2010-2019. Mangrove's cover decreased up to 11% of the total area during these years. The causes of this degradation include reduced river flow, Sea water intrusion, Gradual increase in sea level, Marine and coastal pollution and erosion and meandering of creeks. Sustainability of these mangroves depends on the flooding from Indus Delta which acts as lifeline for their survival.

Table 2.Land Cover Statistics of Indus Delta along Western Indus Delta

Land cover Classes	**Pixel Based Classification (2000)Area Percentage (km²)%**	**Pixel Based Classification (2010)Area Percentage (km²) %**	**Pixel Based Classification (2020)AreaPercentage(km²) %**	**Net change**
Mangroves	279.094402 29.10	395.775923 41.27	306.58 31.97	189.89
Water	215.229175 22.44	349.065464 36.40	374.43 39.04	189.86
Mudflats	405.183777 42.25	71.966799 7.50	251.76 26.25	225.39
Sand	59.368583 6.19	142.079249 14.81	26.096 2.72	-56.61

Total	958.88 100	958.88 100	958.88 100	----------

References

1. Alamgir, M. Impacts of indiscriminate disposal of untreated effluents in Korangicreek,Karachi,Pakistan. Applied Water Science, 2018.
2. Ahmad, F. Mangrove conservation along the coast of Sonmiani, Balochistan, Pakistan. Trees, pp: 213-217, 2002.
3. Ali, N. Flora of Pakistan. Botany Dept. Karachi, University of Karachi, Karachi Vanity Printing Press, 2009.
4. Atta, S. Fragile mangroves and increasing susceptibility to coastal hazards in pakistan. Participatory Mangrove Management in a Changing Climate, pp: 17-30, 2017.
5. Bhim,P. The Use and Management of Mangrove Ecosystem In Pakistan. The Journal of Environment and Development, pp: 446-467, 2010.
6. Chandra Giri, J. Distribution and dynamics of mangrove forests of South Asia. Journal Of Environmental Management, 2010.
7. Stokes, R. Addressing the mismatch between restoration objectives and monitoring needs to support mangrove management. Ocean And Coastal Management, pp:134-146, 2016.
8. Duke, N. Oil spill impacts on mangroves: Recommendations for operational planning and action based on a global review. Marine Pollution Bulletin, pp: 700-715, 2016.
9. Hesham,S. Locating suitable mangrove plantation sites along the Saudi Arabia Red Sea Coast. Journal of African Earth Science, 2013.
10. Masood, S. A. Application of Comparative Remote Sensing Techniques for. Biological Forum – An International Journal, Vol 7, issue 1, pp: 783-792, 2015.
11. Huge, j. Mapping discourses using Q methodology in Matang Mangrove Forest,. Journal of Environmental Management, pp: 988-997, 2016.
12. Khalil, S. THE ECONOMIC VALUATION OF MANGROVES. Pakistan economic and social review, pp: 16-46, 2009.
13. LuojiaHu,L. Monitoring mangrove forest change in China from 1990 to 2015 using Landsat-derived spectral-temporal variability metrics. Int J Apple Earth ObsGeoInformation, 2015.
14. Jayanthi,T. Spatial and temporal changes in mangrove cover across the protected and unprotected forests of India. Esturine,Coastal and Shelf Science, 2017.
15. Oostdijk,J. Assessing rehabilitation of managed mangrove ecosystems using high resolution remote sensing. Estuarine, Coastal and Shelf Science, 2017.
16. Mingming, Z. Monitoring loss and recovery of mangrove forests during 42 years: The achievements of mangrove conservation in China. Int J Appl Earth ObsGeoinformation, pp: 535-545, 2018.
17. Ijaz, b. Geospatial analysis of creeks evolution in the Indus Delta, Pakistan. Estuarine, Coastal and Shelf Science, pp: 324-334, 2017.
18. Ibrahim, N. Mapping mangrove changes in the Matang Mangrove Forest using multi temporal sattlite imageries. Ocean and coastal management, 2015.
19. Bano,N. Significance of bacteria in the flux of organic matter in the tidal creek of the mangrove ecosystembof the indus river delta, Pakistan. Marine Ecology Series, pp:1-12, 1997.

20. Duke, M. Factors influecing Biodiversity and Distributional Gradiants in Mangroves. Global Ecology and Biogeography, pp: 27-47, 1998.
21. Harrison, N. Nutrient and phytoplankton dynamics in mangrove tidal creeks of indus delta, Pakistan. Marine Ecology Progress Series, pp: 13-19, 2006.
22. Qureshi, M. Rehabilitation and management of mangrove forests of Pakistan. Towards the rational of high salinty, pp: 89-95, 2016.
23. Qureshi, T. Experimental Plantation for Rehabilitation of Mangrove Forest in Pakistan. Sindh Forest Department, Government of Sindh, Karachi Pakistan. pp: 86, 1988.
24. Rizvi, S. Status of marine pollution in the context of coastal zone Management in Pakistan. Coastal zone management imperative for Maritime Developing Nations, pp: 347-370, 2015.

OPEN ACCESS
International Journal of Innovations in Science & Technology
IJIST
P ISSN : 2618-1630
E ISSN : 2909-6130

Global temperature variations since pre industrial era

Tariq Noor[1], Iqra Nazeer[2], Zubair Attique[3], Muhammad Shahzad[4]
[1]Institute of social and cultural studies, University of Punjab.
[2] Department of Zoology, University of Education.
[3]University of Lahore.
[4] Department of Computer Science (PUCIT), University of Punjab
* Correspondence: Tariq Noor[1] (noor.tariq36@gmail.com).
Citation | Noor. T, Nazeer. I, Attique. Z, Shahzad. M "Global temperature variations since pre industrial era". International Journal of Innovations in Science & Technology, Vol 03 Issue 02: pp 67-73, 2021.

Received | April 14, 2021; Revised | May 01, 2021; Accepted | May 06, 2021; Published | May 10, 2021.

Abstract.

The global temperature trends are being changed due to anthropogenic activities. The natural ecosystems and human societies are affected by this rapid climate change. These changes are caused by the increasing concentration of carbon dioxide and other greenhouse gases including methane and oxides of nitrogen and Sulphur. These changes can be identified using accurate data related to variations in temperature and precipitation. We used MODIS GLOVIS LST V6 global datasets to compute pixel-based temperature and mapped the trends. The considerable warming trends are exhibited by Arctic regions which are warming twice as compared to other parts of world. The largest increase in precipitation occurred in Northern Europe at rate of 12.9mm per decade. The concentration of carbon dioxide has been raised up to 4.14 ppm in atmosphere by December 2020. This increased concentration has raised the global temperature up to 1.2°C since pre industrial era. Remotely sensed datasets provided promising results.

Keywords: Global temperature, Greenhouse gases, pre industrial era, warming trends, carbon dioxide.

Introduction

Globally, it has been observed that the climate change due to anthropogenic activities caused an increase in concentration of atmospheric carbon dioxide (CO_2) and other gases. Earth's climate has been changed dramatically since 19th century [1]. This climate change contributed to variations in solar energy patterns received and reflected by earth, temperature trends and glacial ice melting. The global mean surface temperature has been increased up to 1.18°C since 19th centaury estimated by linear trend according to the Fourth Assessment Report of the Intergovernmental Panelon Climate Change (IPCC-AR4) [2,3].

Wave transform method and Mann–Kendall rescaled range method for analysis of periodic properties and global trends of precipitation and air temperature from 1948 to 2010. The results show that about 65.34% of total area exhibits warming trend while 3.18%ofthearea show cooling trends [4]. The considerable warming trends are exhibited by Antarctica and Middle Africa which are 0.32 °C per decade and 0.21°C per decade respectively. The dry and wet trends are shown by 22.01% and 62.26 % respectively. The largest increase in precipitation occurred in Northern Europe at rate of 12.9mm per decade [5].

Various nonparametric and parametric techniques have been devised during past decade in order to detect long term trends of temperature and precipitation in time series. Parametric factors show the probability distribution of random variables while nonparametric tests do not exhibit probability distribution. For the hydro meteorological time series analysis the nonparametric tests are usually encountered [6]. According to global temperature indicator, rise in surface temperature caused the evaporation which triggers rise in precipitation [7]. The precipitation rate changes the climatic conditions by effecting rainfall, timing of snow melt and by shifting wind patterns. Moreover, higher the temperature, greater will be the evaporation which can lead to droughts by decreasing the amount of water on the surface of earth. Precipitation has also increased since 1900 to 2005 over 30° N while precipitation level is decreased in tropics since 1970s [8].

This alarming change in temperature occurred due to increased concentration of Carbon dioxide and other greenhouse gases in atmosphere. These gases include methane, oxides of nitrogen and Sulphur which have the ability to trap heat thus raise the temperature of atmosphere [9]. The concentration of these gases is rising 250 times faster due to anthropogenic activities rather than their natural resources. The concentration of carbon dioxide increased up to 40% after the evolution of industries. The concentration increased from 280 to 415 ppm from 1850 to 2019 [10].

Natural ecosystems as well as human localities have been affected considerably by climate change. The climate change detection requires accurate information regarding the space-time distribution of temperature and precipitation. Global increase in temperature triggers expansion of forest fires, deserts and heat waves [11]. The warming of Arctic region resulted in the loss of Arctic ice, glacial retreat and rise of sea level. Global rise in temperature also triggered extreme weather conditions and storms due to increased rate of precipitation [12].

During the year 2018, nearly 52 billion tons of greenhouse gases has been added to atmosphere via anthropogenic activities. Among these gases, 72% carbon dioxide was emitted, methane contributed 19%, and nitrous oxide was added up to 6% while fluorinated gases contributed 3%. Burning of fossil fuels, industrial processes, electricity production and deforestation contributed to the concentration of carbon dioxide in atmosphere [13].

Global variation in temperature has affected the environment adversely, for increasing wind speed, rainfall and typhoons in Asian regions. In Antarctica, the sea level is rising due to melting of glaciers and ice caps leading to temperature expansion [14].

The main purpose of this research was to examine the temporal expansion of heat island with respect to equator. It also aims at appraising the aftermath of

dramatic increase of atmospheric gases globally.

Material and Methods

The datasets used in this research include MODIS GLOVIS LST V6, downloaded from earth explorer website (https://earthexplorer.usgs.gov/) for the years from 2000 to 2020. Each dataset is comprised of pixel-based temperature values. The reflectance of each pixel was converted to temperature using the following formula,

Temperature = (Irradiance * 0.02)-273

We obtained the concentration of various gases including (CO_2, NO_2 and CH_4) from GIOVAANI for the years from 2000 to 2020. These concentrations are helpful to understand, how atmospheric gases contribute in trapping of reflected heat which caused global warming.

Results and Discussions.

The temporal change in temperature from 2000 to 2020 is mapped in Figure 1 as below,

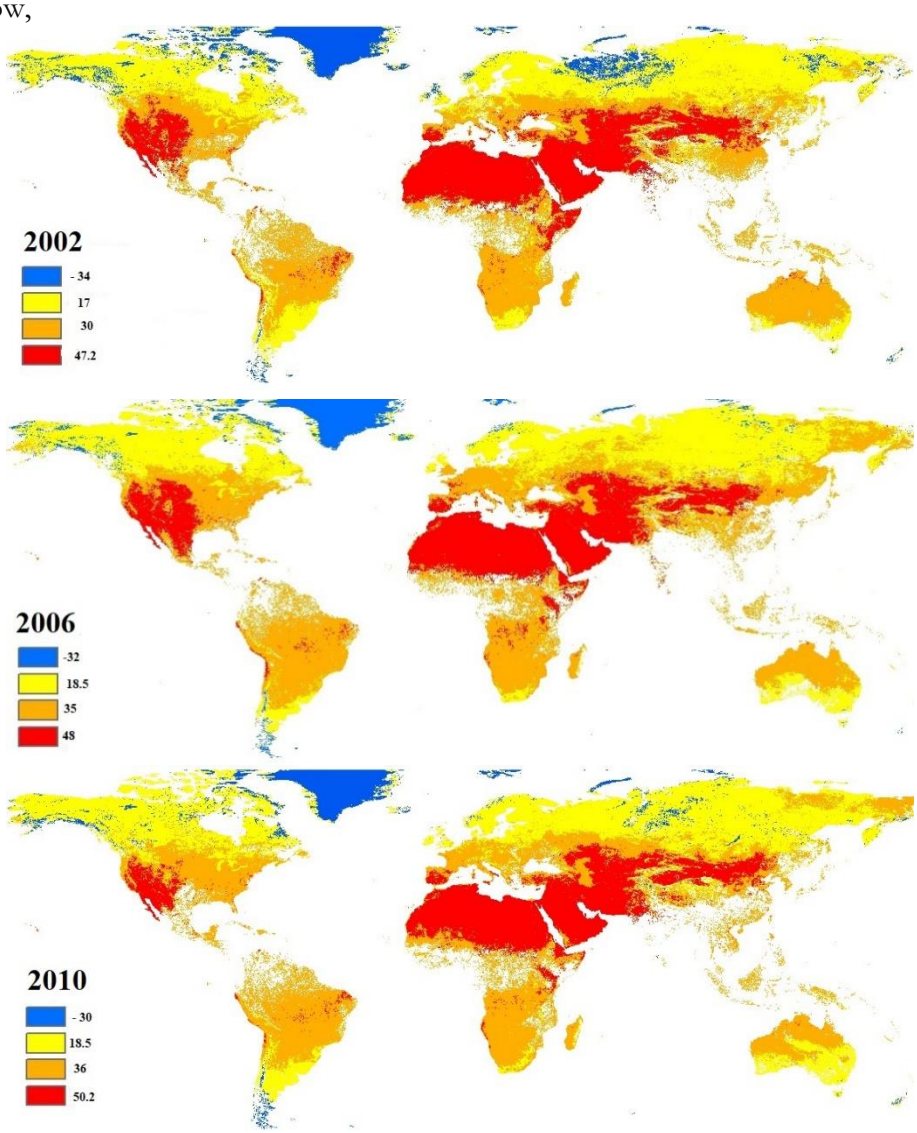

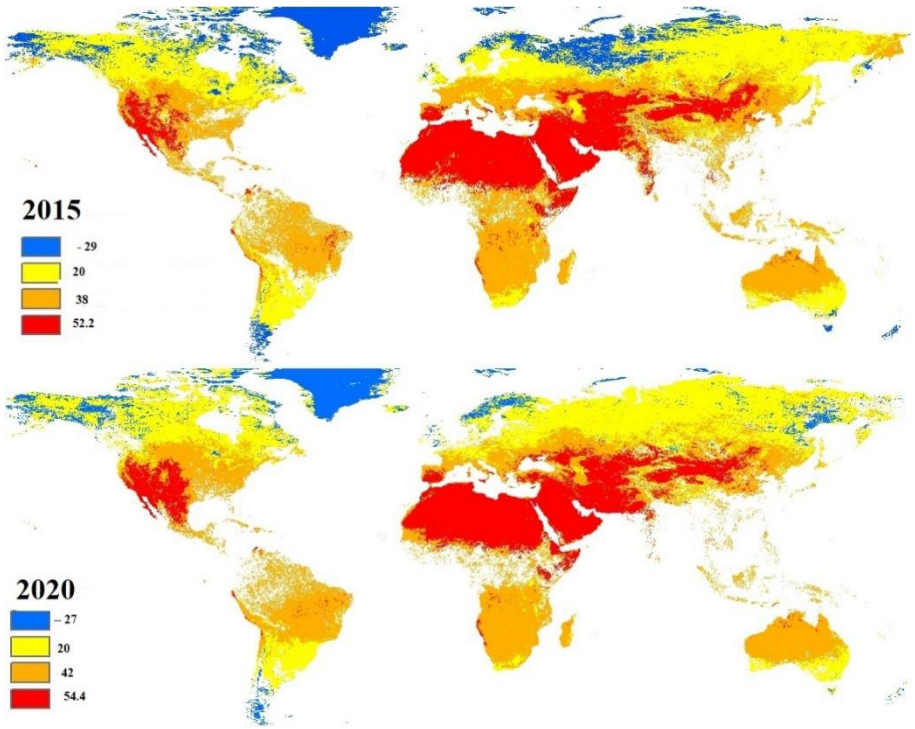

The temperature rise is not uniform globally but according to Annual Climate Report of NOAA, since 1880 the temperature has been increased at the rate of 0.08°C per decade. The temperature in Arctic regions of world has increased three times faster than other parts of the world. Due to this warming trend, the Arctic ice is decreasing at the rate of 13% per decade. The Arctic region has been warmed twice as compared to other parts of word over last 30 years in a process of Arctic amplification. Arctic oceans absorb more heat leading to more warming of the region. Figure 2 shows the loss of ice mass due to global warming.

Global temperature has been increasing for decades but the years 2014-2018 were considered the hottest years of decade since 1980. Annual and five-year temperature anomalies are shown in Figure 3. These years face 1°C rise in temperature as compared to the previous years. According to NASA, the year 2018 was the fourth warmest year since 1980. The average global temperature rose up to 0.83°C higher than the mean temperature in the year 1980. This warming caused melting of glaciers and polar snow which raised water level in sea which contributed to floods, droughts and long-lasting forest fires.

According to the NASA, HadCRUT and NOAA, the temperature of the year 2020 raised up to 1.2°C as compared to the temperature of pre-industrial area (1880). Figure 5 shows the global temperature range for the year 2020. This alarming rise in temperature is due to increase in concentration of carbon dioxide in atmosphere.

The concentration of carbon dioxide has been raised up to 4.14 ppm in atmosphere by December 2020. The increase in concentration of CO_2 is a leading cause of global warming. The Figure 5 shows the rise in concentration of greenhouse gases in atmosphere.

The figure 5 shows that the concentration of CO_2, NO_2 and CH_4 has increased significantly since evolution of industries, where the concentration of CO_2 increased from 280ppm to 415 ppm by the year 2020, while the concentration of methane has increased up to 2000ppb by the year 2020. For instance, methane and oxides of nitrogen and Sulphur have been increased to an alarming level since the evolution of industries in the world. The more the concentration of greenhouse gases, more heat will be trapped causing a global rise in temperature and increasing the precipitation and trends of evaporation. Figure 6 shows the global trend of precipitation globally.

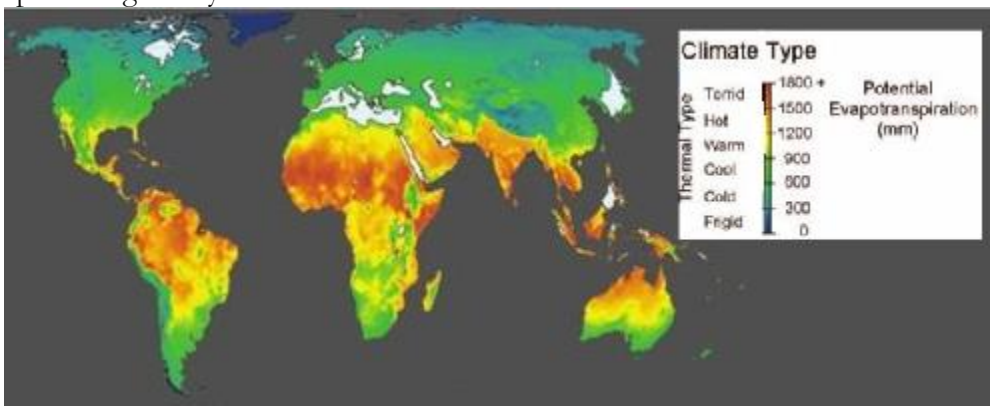

Figure 6: Global precipitation trend (mm)

Figure 1. shows that the fluctuations in global temperature are 0.93 ± 0.07 °C from the years 2009-2020. The temperature of surface of Earth is rising nearly 0.2 °C per decade. The temperature of the year 2020 has increased up to 1.2°C as compared to the temperature of pre industrial area (1880). Thus, due to larger heat capacity of water oceans has trapped 90% of the solar energy. However, the oceanic circulation in Arctic region has been disrupted due to the rapid ice and glacier melting.

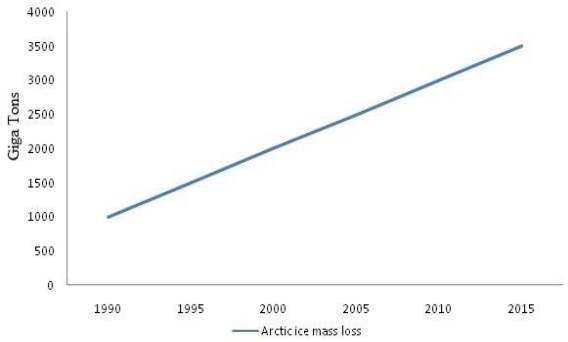

Figure 2. Arctic loss of ice due to global climate change

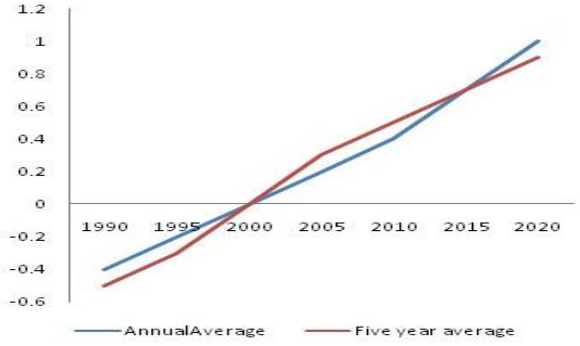

Figure 3. Average annual and five years temperature anomalies.

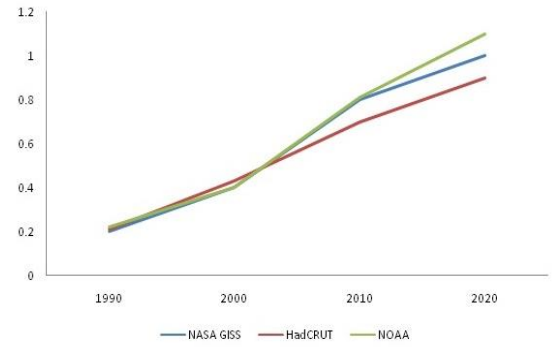

Figure 4. various indicators portraying the average rise in temperature over the globe

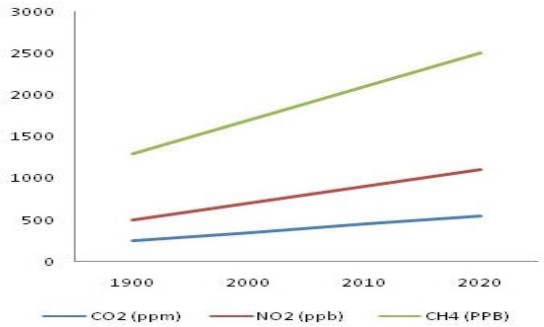

Figure 5. shows the concentration of green house gases in atmosphere along the temperature range for the year 2020.

Conclusion

The climate is affected by both natural and anthropogenic factors but since 19th centaury human activities have affected the temperature trend over a global scale. During the year 2018 nearly 52 billion tons of greenhouse gases has been added to atmosphere via anthropogenic activities. The concentration of carbon dioxide has been raised up to 4.14 ppm in atmosphere by December 2020. Thus, the increased concentration of carbon dioxide and other greenhouse gases have raised the temperature of earth to an alarming level. Temperature rise has resulted in melting of glaciers, increased sea level, flood outbursts and longer wild fires.

Conflict of Interest.

The authors declare no conflicts of interest regarding the publication of this paper.

Project Detail. Nil

References

1. Abghari,H.,Tabari,H.,&Talaee, P.H.(2013).Riverflowtrends in the west of Iran during the past 40 years: impact of precipitation variability. Global and Planetary Change, 101, 52–60.
2. Alexander,L.V.,Zhang,X.,Peterson,T.C.,Caesar,J.,Gleason, B.,Tank,A.M.G.K.,etal.(2006).Globalobservedchanges in daily climate extremes of temperature andprecipitation. JournalofGeophysicalResearch,111,D05109.
3. Ambenje,P.,etal.(2007).InS.Solomon,D.Qin,M.Manning,Z. Chen,M.Marquis,K.B.Averyt, M.Tignor,&H.L.Miller (Eds.), IPCC, 2007: climate change 2007: the scientific basis.ContributionofworkinggroupItothefourthassess-ment report of the inter-governmental panel on climate change(p.243).Cambridge:CambridgeUniversityPress.
4. T. Westerhold et. al., "An astronomically dated record of Earth's climate and its predictability over the last 66 million years," Science vol. 369 (11 Sept. 2020), 1383-1387.
5. "Scientific Consensus: Earth's Climate is Warming". Climate Change: Vital Signs of the Planet. NASA JPL. Archived from the original on 28 March 2020. Retrieved 29 March 2020.; Gleick, 7 January 2017.
6. "The State of the Global Climate 2020". World Meteorological Organization. 14 January 2021. Retrieved 3 March 2021.

7. PCC, 2013b: Summary for Policymakers. In: Climate Change 2013: The Physical Science Basis. Contribution of Working Group I to the Fifth Assessment Report of the Intergovernmental Panel on Climate Change [Stocker, T.F., D. Qin, G.K. Plattner, M. Tignor, S.K. Allen, J. Boschung, A. Nauels, Y. Xia, V. Bex, and P.M. Midgley (eds.)]. Cambridge University Press, Cambridge, United Kingdom and New York, NY, USA, pp. 3–29.
8. IPCC, 2012a: Summary for Policymakers. In: Managing the Risks of Extreme Events and Disasters to Advance Climate Change Adaptation [Field, C.B., V.R. Barros, T.F. Stocker, D. Qin, D.J. Dokken, K.L. Ebi, M.D. Mastrandrea, K.J. Mach, G.-K. Plattner, S.K. Allen, M. Tignor, and P.M. Midgley (eds.)]. Cambridge University Press, Cambridge, United Kingdom and New York, NY, USA, pp. 3–21.
9. IPCC, 2014a: Summary for Policymakers. In: Climate Change 2014: Impacts, Adaptation, and Vulnerability. Part A: Global and Sectoral Aspects. Contribution of Working Group II to the Fifth Assessment Report of the Intergovernmental Panel on Climate Change [Field, C.B., V.R. Barros, D.J. Dokken, K.J. Mach, M.D. Mastrandrea, T.E. Bilir, M. Chatterjee, K.L. Ebi, Y.O. Estrada, R.C. Genova, B. Girma, E.S. Kissel, A.N. Levy, S. MacCracken, P.R. Mastrandrea, and L.L. White (eds.)]. Cambridge University Press, Cambridge, United Kingdom and New York, NY, USA, pp. 1–32.
10. Mysiak, J., S. Surminski, A. Thieken, R. Mechler, and J. Aerts, 2016: Brief communication: Sendai framework for disaster risk reduction – Success or warning sign for Paris? Natural Hazards and Earth System Sciences, 16(10), 2189–2193, doi:10.5194/nhess-16-2189-2016.
11. IPCC, 2012a: Summary for Policymakers. In: Managing the Risks of Extreme Events and Disasters to Advance Climate Change Adaptation [Field, C.B., V.R. Barros, T.F. Stocker, D. Qin, D.J. Dokken, K.L. Ebi, M.D. Mastrandrea, K.J. Mach, G.-K. Plattner, S.K. Allen, M. Tignor, and P.M. Midgley (eds.)]. Cambridge University Press, Cambridge, United Kingdom and New York, NY, USA, pp. 3–21.
12. Albert, S. et al., 2017: Heading for the hills: climate-driven community relocations in the Solomon Islands and Alaska provide insight for a 1.5°C future. Regional Environmental Change, 1–12,
13. IPCC, 2014a: Summary for Policymakers. In: Climate Change 2014: Impacts, Adaptation, and Vulnerability. Part A: Global and Sectoral Aspects. Contribution of Working Group II to the Fifth Assessment Report of the Intergovernmental Panel on Climate Change [Field, C.B., V.R. Barros, D.J. Dokken, K.J. Mach, M.D. Mastrandrea, T.E. Bilir, M. Chatterjee, K.L. Ebi, Y.O. Estrada, R.C. Genova, B. Girma, E.S. Kissel, A.N. Levy, S. MacCracken, P.R. Mastrandrea, and L.L. White (eds.)]. Cambridge University Press, Cambridge, United Kingdom and New York, NY, USA, pp. 1–32.
14. Dryzek, J.S., 2016: Institutions for the Anthropocene: Governance in a Changing Earth System. British Journal of Political Science, 46(04), 937–956.
15. Pattberg, P. and F. Zelli (eds.), 2016: Environmental politics and governance in the Anthropocene: Institutions andlegitimacy in a complex world. Routledge, London, UK, 268 pp.

OPEN ACCESS International Journal of Innovations in Science & Technology

IJIST
P ISSN : 2618-1630
E ISSN : 2909-6130

Novel Technique to Investigate Glacio-fluvial Hypsometry in Hunza Using Local Indicator of Spatial Autocorrelation (LISA)

Syed Amer Mahmood[1], Sarah Hassan[2], Hania Arif[3], Saira Batool[4], Areeba Amer[5], Muhammad Shahazad[6] Rana Muhammad Sohail Aslam[7], Bushra Talib[8]

[2,5]Center For Integrated Mountain Research (CIMR), University of the Punjab, Lahore.
[3,4]College of Earth and Environmental Sciences (CEES), University of the Punjab, Lahore
[1,7] Department of Space Science, University of the Punjab, Lahore
[8]Department of Technology & engineering, University of the Lahore.
[6] Department of Computer Science (PUCIT), University of Punjab
* Correspondence: Syed Amer Mahmood (amerpakistan@gmail.com)
Citation | Mahmood. A, Hassan. S, Batool. Arif. H, "Novel Technique to Investigate Glacio-fluvial Hypsometry in Hunza Using Local Indicator of Spatial Autocorrelation (LISA)". International Journal of Innovations in Science & Technology, Vol 03 Issue 02: pp 73-85, 2021.
Received |May 11, 2021; Revised | May 28, 2021; Accepted | June 04, 2021; Published | June 09, 2021.

Abstract

Hypsometric Integral (HI) displays the effect of active tectonics and sensitivity on geomorphic structures. In this study we calculated HI values for Hunza valley to investigate neotectonics, development of topographic structures and process of erosion using SRTM DEM 90m. ArcGIS and MATLAB is used to generate HI and hypsometric curve (HC). We generated HI and HC values by using D8 algorithm in MATLAB to extract drainage basins for 5 and 6 Strahler orders. HI and HC values show the stages of erosion for instance high values of HI and convex HC displays young and tectonically active stage. We used different grid sizes in ArcGIS to calculate maximum, mean and minimum elevation utilizing different statistical techniques. We used Local Indicator of Spatial Autocorrelation (LISA) instead of Global Moran Index to determine the extent of distribution of clustered, dispersed and randomized HI values. This technique indicates high positive z score for auto correlated data. Regions with high HI value indicate relative uplift, undissected and young structures while low HI values indicate sediment accumulation and shallow earthquakes.

Keywords: SRTM DEM 90m, Global Moran Index, Hypsometry, Spatial auto-correlation.

Introduction

Hunza valley is a mountainous region situated in the northern zone of Gilgit Baltistan. The Precambrian aged rock of Hunza comprises of metamorphic and igneous rocks. The rocks

in Hunza are identified on the basis of age. Hunza also comprises of the corundum [1]. Hunza comprises of two major tectonic features including Main Karakoram Thrust and Main Mantle Thrust.
Nearly 36000 km^2 region of MKT and MMT covers almost plutonic, subordinate sedimentary, volcanic, metamorphosed and deformed rocks. Both tectonic regions display an arc of intra oceanic island developed from the subduction of northward oceanic lithosphere [2]. The study of active tectonics is considered the most advanced tool used for the analysis of hazards and populated areas.
The geography of earth comprises of active tectonics, geographic structures and climate [3]. The geomorphology has emerged along multiple disciplines including geomorphology, geodesy, stratigraphy, geochronology, and seismology. The remote sensing techniques are used in these geomorphologic studies [4].
Hypsometric Integral (HI) displays the effect of active tectonics and sensitivity on geomorphic structures [5]. In this study we computed HI values for Hunza valley to investigate neotectonics, development of topographic structures and process of erosion using SRTM DEM 90m. ArcGIS and MATLAB is used to generate HI and Hypsometric Curve (HC) [6].
The ratio between cross section area and elevation is given by Hypsometry [7]. The area under hypsometric curve provides the value of hypsometric curve. Hypsometrically obtained data determines steps and processes of reshaping of different structures with respect to time within the defined area or natural drainage basins [8,9].
The hypsometric analysis is vital indicator of condition of watershed. It has two components including "*Hypsometric Curve*" and "*Hypsometric Index*".HI has strong association with basin geometry, drainage area and elevation of the basin [10]. HI is independent of drainage area while it is associated with relative rate of uplift. It is scale dependant tool which may be affected by climate, lithology and tectonics [11].
Variations in glaciated terrain depend upon hypsometry, the equilibrium line altitude (ELA) moves due to changing climate [12]. According to the geometry of glacier the accumulation area and ablation of glacier change due to changing elevation. Contrariwise only a small area at the ELA being large in its height may have little variation [13].
Moreover, glaciers having similar ELA exhibit quite different behavior. One glacier with broad accumulation area and a narrow snout while other glacier with narrow upper basin and a wide tongue [15]. The percentage of area of ablation and accumulation zone of glacier can be computed by plotting ELA on HC. It also calculates the variations with respect to time [16].
SRTM DEM 90m was used to compute hypsometric integral (HI). The LISA technique is also used to calculate low and high values of HI clusters [17]. The process of erosion, climatic variations, active tectonics and lithological features of basin are determined by the shape of curve in HC.

Study Area

Hunza is a mountainous region located in the northern zone of Gilgit Baltistan. The Hunza basin is situated in the central region of Karakoram. The basin lies within the 35° 54' to 37° 05' latitude and 74° 02' to 73° 03 longitude respectively. The basin comprises of Gilgit River in the western side, China and Afghanistan in the northern zone, and Indus River and Shigar River in the southern zone. Naltar, Nagar, Shimshal and Chapursan are the major valley of

the basin (Figure 1). The basin covers 16,389.4 km^2 out of which Hunza River comprises of 87.5% flow [18].

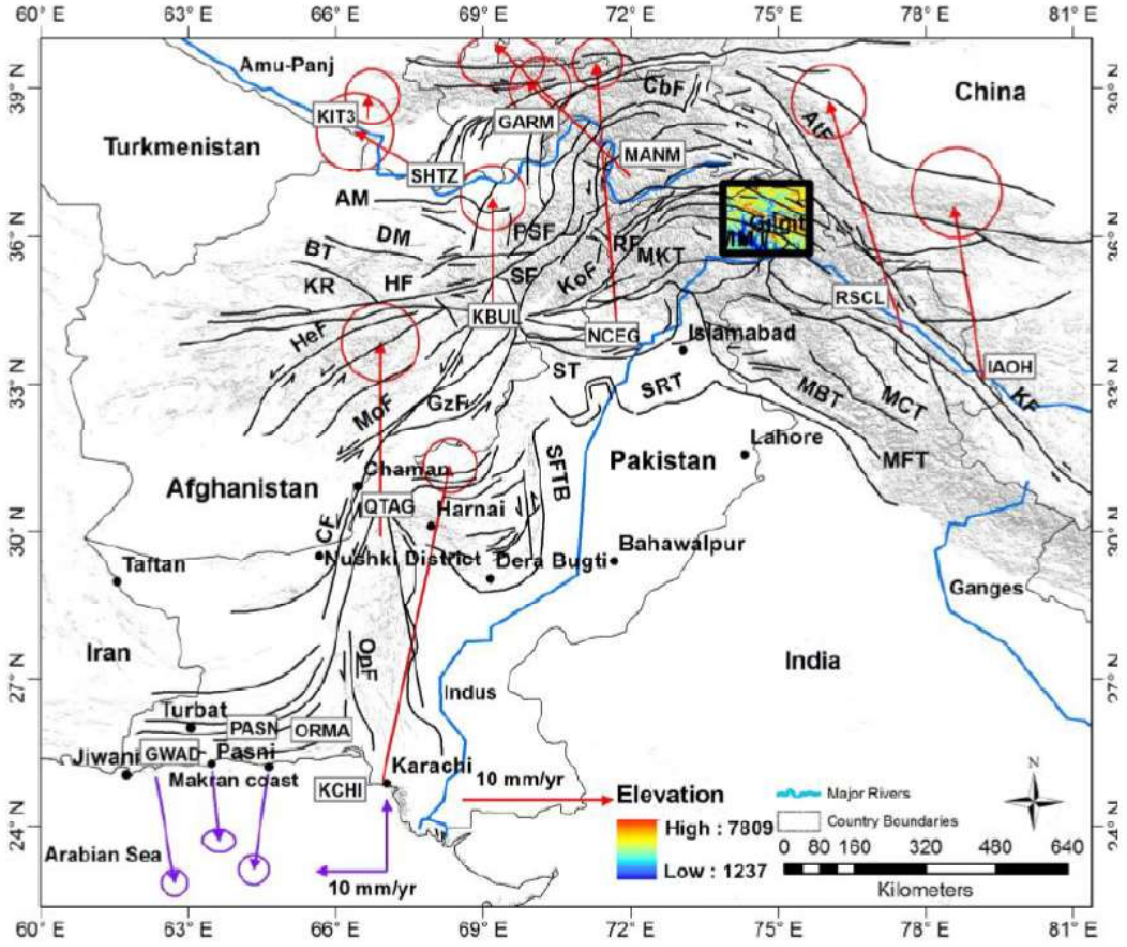

Figure 1. Diagram showing regional tectonics in the context of Indo-Pak-Eurasian collision.

Materials And Methods

Different grid sizes are required in SRTM DEM 90m to determine HI. SRTM DEM 90m is obtained from http://srtm.csi.cgiar.org/SELECTION/inputCoord.asp.The DEM is precise technique which covers almost all regions of the world. Nearly 16m vertical error occurs in DEM. ArcGIS fills the DEM sinks. Zonal statistics calculates the values of HI for different square grids [19]. It also computes minimum, maximum and mean value of elevations in DEM (Figure 2, 3). The obtained values of HI indicate variations of grid squares with respect to glacial, tectonic and lithological boundaries (Figure 4,5). Due to complexity of landscape both low and high values of HI can appear on the basis of grid squares [20].

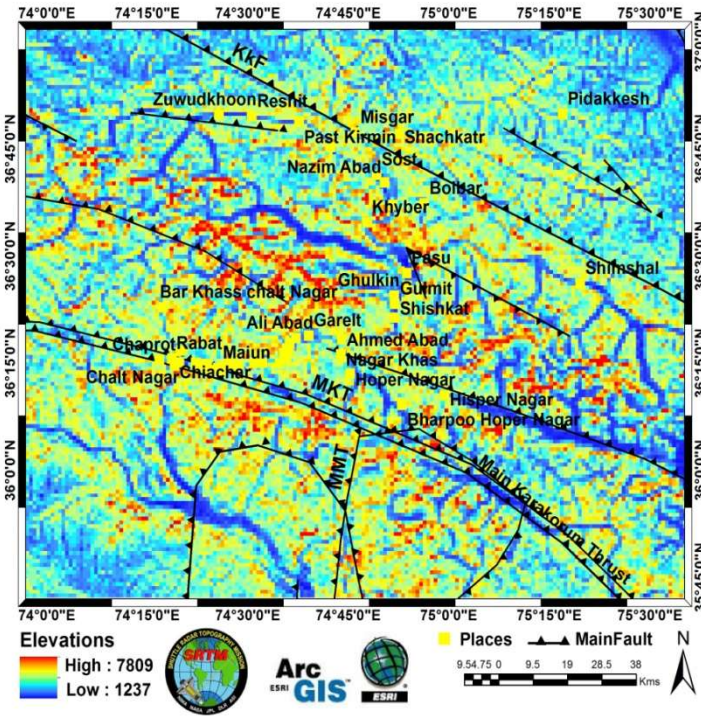

Figure.2 Digital Elevation Model (DEM) of 90 m resolution of the Hunza and adjacent regions showing faults and main rivers.

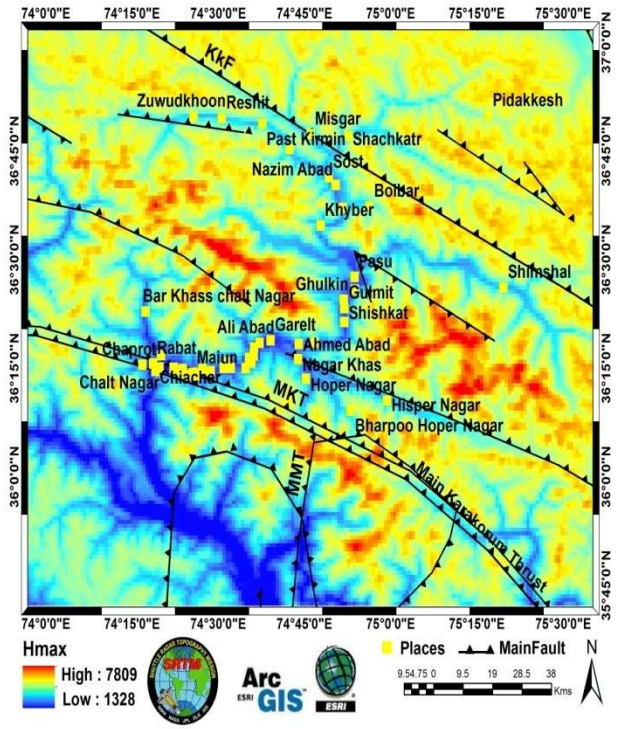

Figure. 3 Map showing spatial distribution of HI maximum values for the Hunza and its outskir

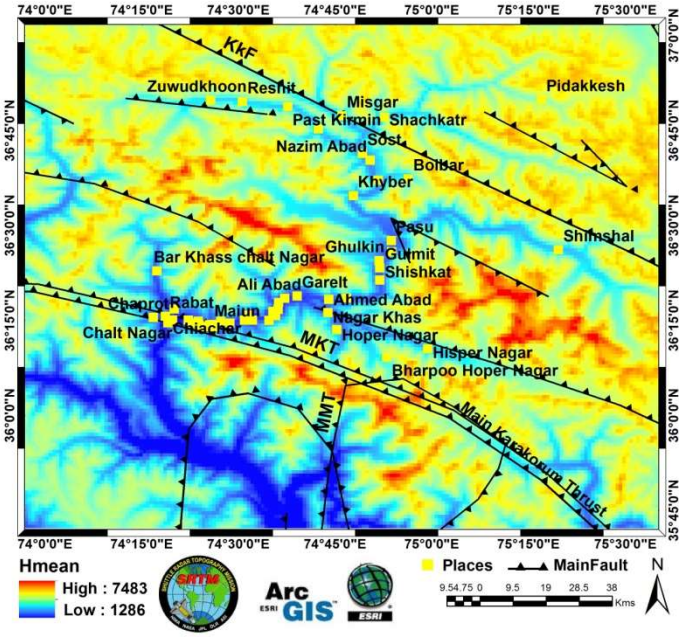

Figure.4Map showing spatial distribution of HI mean values for Hunza and its outskirts.

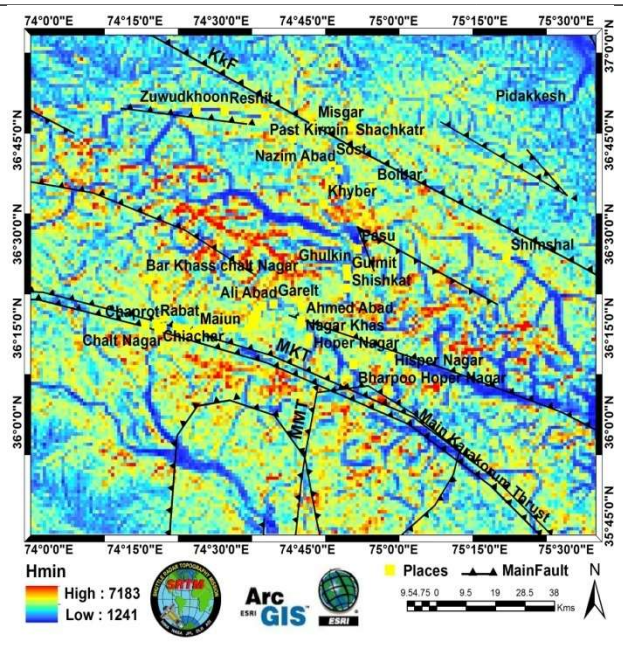

Figure. 5Map showing spatial distribution of HI minimum values for Hunza and its outskirts.

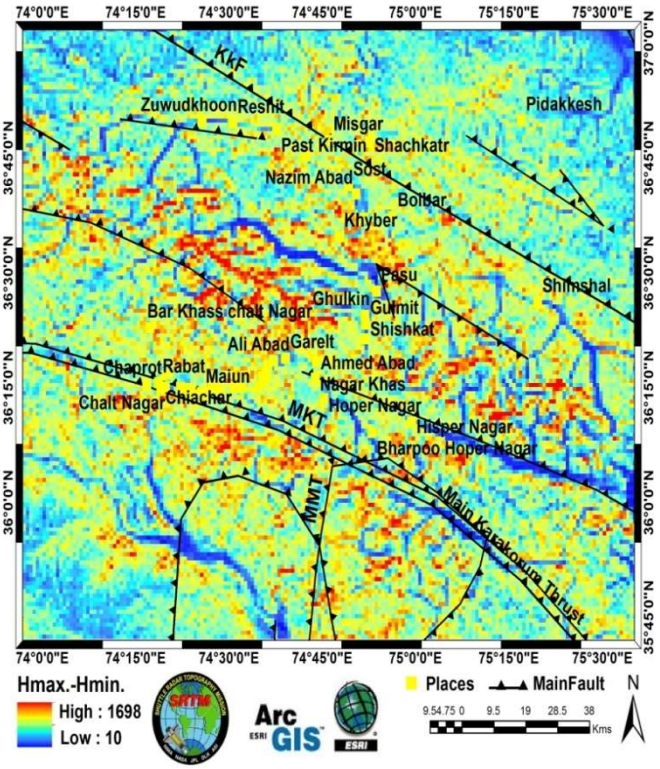

Figure. 6Map showing spatial distribution of Hmax-Hmin values for Hunza and its outskirts.

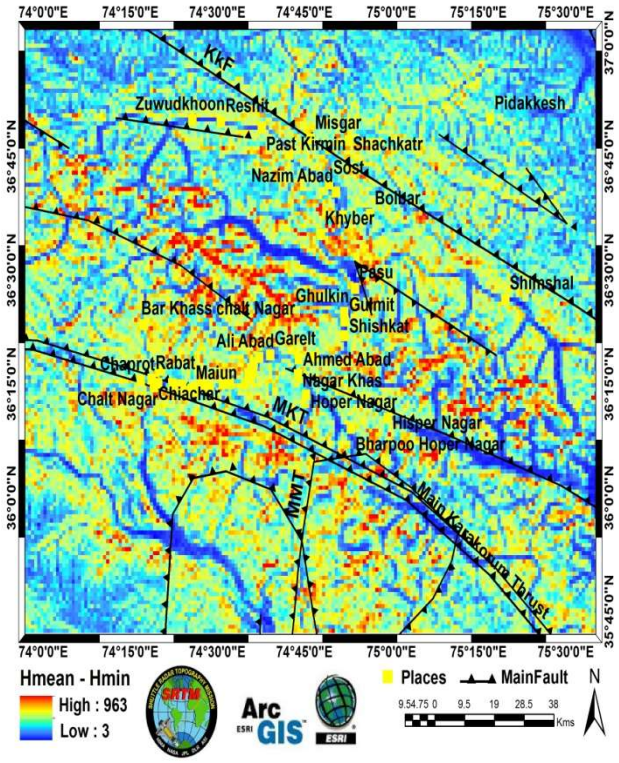

Figure. 7Map showing spatial distribution of Hmean-Hmin values for Hunza and its outskirts.

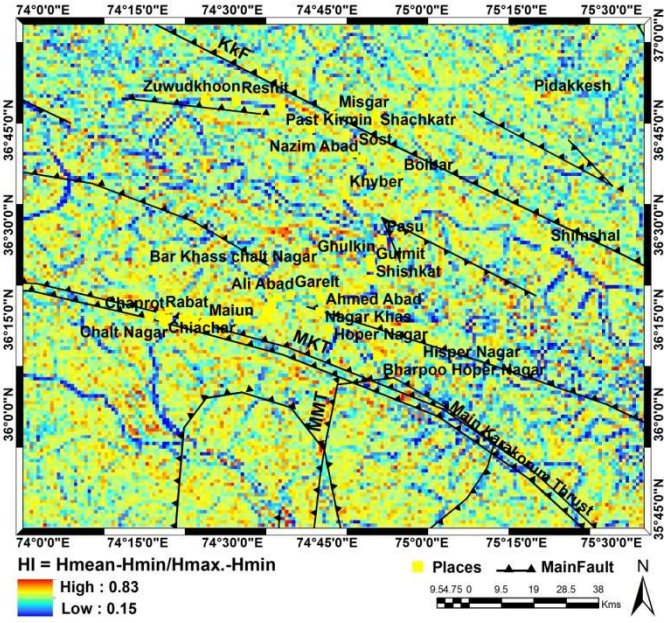

Figure.8Map showing $HI=\frac{H_{mean}-H_{\min}}{H_{\max}-H_{\min}}$ values for Hunza and its outskirts.

Moran Index

In order to obtain the spatial distribution of HI we apply spatial autocorrelation. The spatial autocorrelation and its association are determined in geologically referenced datasets using spatial statistical analysis [21]. Figure 9. Shows the schematic illustration of cells with different HI values due to change in altitude variations depending only on the location of the cells.

$$HI = \frac{H_{mean} - H_{min}}{H_{max} - H_{min}} \quad (1)$$

Moran I index is an accurate tool which computes the spatial autocorrelation precisely. This tool determines the dispersed, random and clustered cell values. This method correlates the observations using following formula.

$$I = \left[\frac{N}{\sum_i \sum_j w_{ij}}\right]\left[\frac{\sum_i \sum_j w_{ij}\,(x_i - \bar{x})(x_j - \bar{x})}{\sum_i (x_i - \bar{x})^2}\right] \quad (2)$$

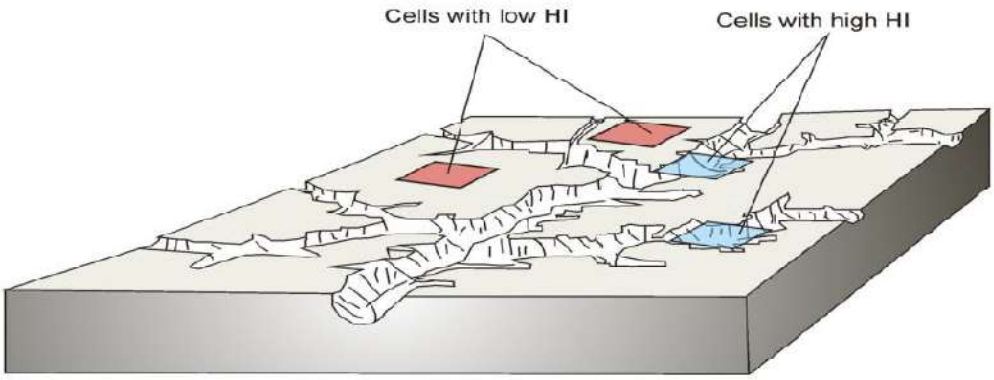

Figure 9. Schematic illustration showing cells with different HI values due to change in altitude variations depending only on the location of the cells.

Where, N represents the number of observations, i,j shows the rows and column of the matrix, w_{ij} shows the spatial weighted matrix (SWM) for each observation cells (i,j), and x_i and x_j are the observations for the i and j location (with mean).

LISA application

GMI method provides average variation and limited association of spatial autocorrelation. LISA technique overcomes this limitation. This technique displays the spatial independence data [22]. This tool is useful for the observation of spatial clustering of global cold and hot spots at different locations. The Moran index is standard tool to determine autocorrelation while LISA explores the association among observations [23]. Specific spatial autocorrelation can be measured using the following equation.

$$Gi^* = \frac{\sum_j w_{ij}(d) x_j}{\sum_j x_j} \quad (4)$$

Where, W_{ij} (d) is a weight index of i location with respect to j.

Results and Discussion

Hypsometric Analysis Basin wise

Hypsometric curve and hypsometric integral are computed for Strahler order 5 and 6 in MATLAB for Hunza sub-basins. The obtained values of HC are s shaped, concave in downward direction and convex in upward direction. The Hypsometric curve indicates different stages of erosion, active tectonics and relative rate of uplift. The high HI values are characterized by convex up of HC. It also characterizes the less corrosive regions and high topography which is under development.

Low HI values are indicated by downward concave HC (Figure 11). It also portrays erosion, old stages and even dissection of drainage sub basins. The HI values are normally distributed up to an average mean of 0.25. Distribution of HI does not display clear spatial pattern because of variations in local topography (Figure 10).

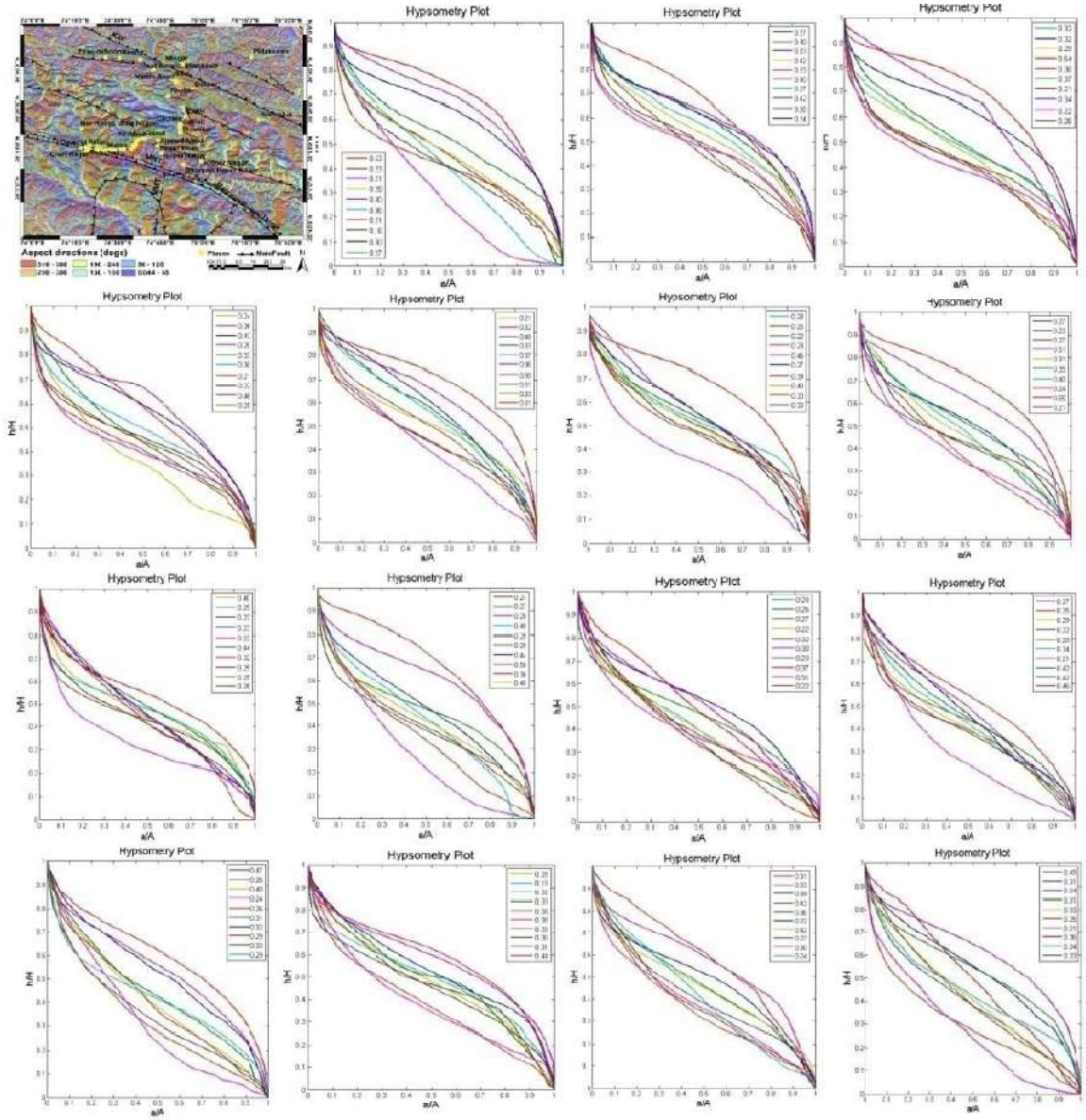

Figure 10. Illustration showing aspect map and hypsometric curves for the subbasin of order 4.

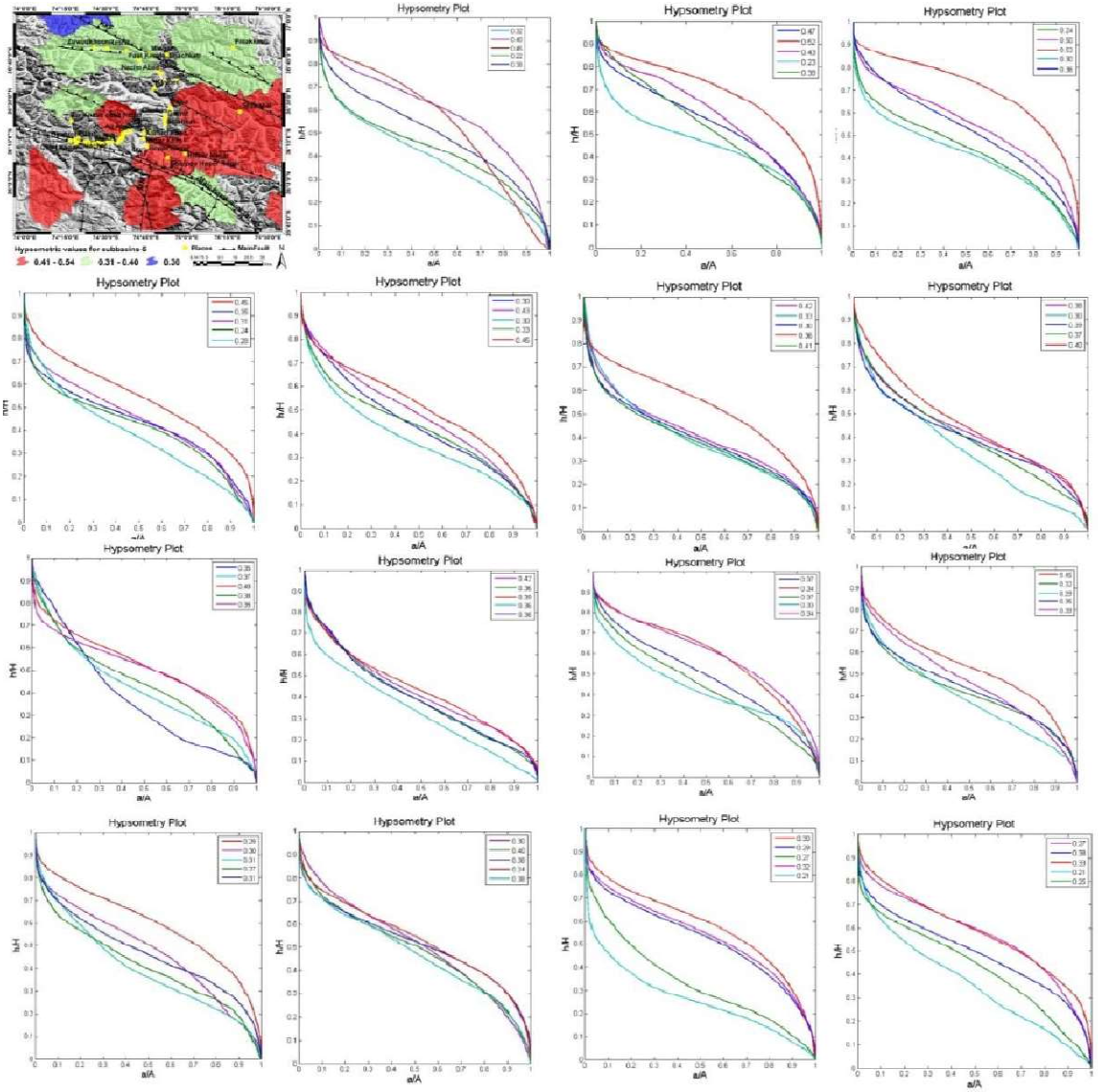

Figure 11. Illustration showing map and hypsometric curves for the subbasin of order 5.

Hypsometric Analysis grid wise

The Moran Index statistics detects the distribution of HI spatial pattern of autocorrelation Table 1 represents Moran Index, Expected Moran Index and z score for each dataset. Figure 12. showsGetisord G* statistics for various analysis grid sizes (1Km, 2Km and 3 Km) for a fix band distance (FBD) of 3Km.

Table 2 Results of Moran Index for 90m DEM with different analysis square grid

DEMs	Analysis Grid	*N*	*I*	*E(I)*	*Z*	*P*
90 m	1 km	27267	0.178190	-0.000040	53.624647	0.000000
90 m	2 km	6808	0.184567	-0.000159	27.730756	0.000000
90 m	3 km	3100	0.220772	-0.000346	16.558362	0.000000
90 m	4 km	1739	0.190144	-0.000614	10.515920	0.000000

High value of z-score shows the clustering of the data.

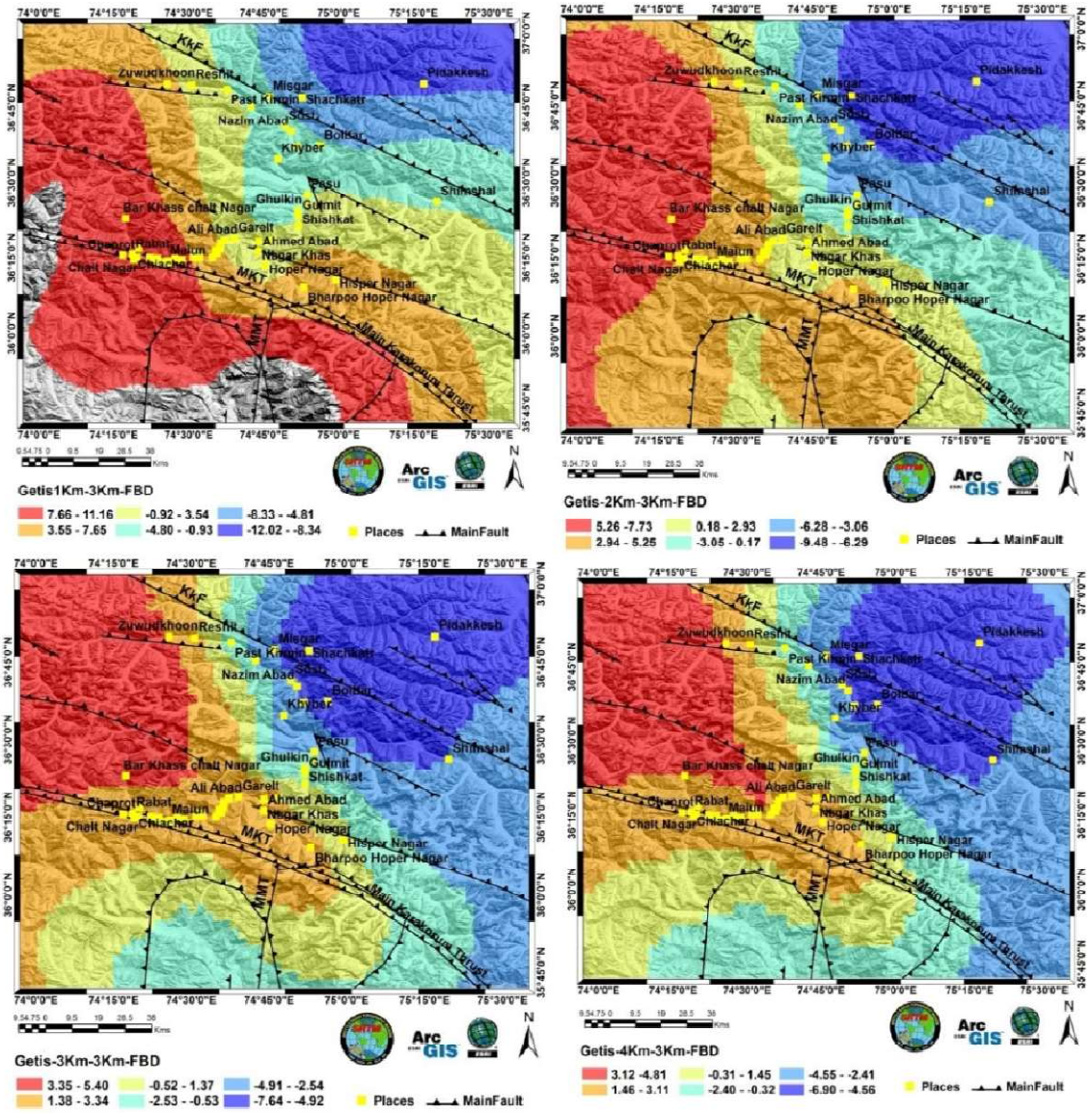

Figure 12. Map showing Getisord G* statistics for various analysis grid sizes (1Km, 2Km and 3 Km) for a fix band distance (FBD) of 3Km

Discussion

Spatial Dependency of scale

The global Moran I statistics display autocorrelation of HI observations.. HI datasets comprises of high positive values of z scores. The resolution of DEM decreases at different spots by increasing the grid size. The LISA technique is applied using different grid sizes; grids covered different areas although the display remained the same. The value of Z score is inversely proportional to the grid size i.e, it decreases by increasing the size of grid. The Z score exhibits scale dependency of spatial patterns of auto correlation.

Neotectonics and correlation to HI values

The result shows that the red zones and the high values of HI are distributed spatially towards northern east and southern west region of Hunza. They are most significantly distributed along northern east along MKT and MMT faults where relative rate of uplift is high. These faults are has hosted a number of intermediate, shallow and deep earthquakes. The regions with low values of HI are spatially distributed around Gulkin, Passu, Nazim Abad, Bolbar, Sost, Khyber, Shiskat, Misgar, Gulmit, Pidakkesh and Shachkatr which have sediment deposits, shallow earthquakes, fault traces and tectonically active areas.

Conclusions

Hunza valley is a mountainous region situated in the northern zone of Gilgit Baltistan. Analysis and techniques were applied over Hunza valley to illustrate that Global Moran Index (GMI) is a precise tool to compute and locate the spatial patterns in SRTM DEM 90m based datasets. It is observed from the results of GMI that HI values are distributed spatially in the form of low and high values. GMI method provides average variation and limited association of spatial autocorrelation. LISA technique overcomes this limitation. This technique displays the spatial independence data. Both these techniques illustrate that values of HI depend upon the scale. The high HI value indicates active faults and active tectonics while low value of HI indicates shallow earthquakes and sediment deposition.

Acknowledgment

The authors are thankful to the of department of Space Science, University of the Punjab, Lahore Pakistan, for providing necessary provisions regarding GIS and RS related issues and Lab. support.

Refrences

1. Eyles, N. and Scheidegger, A. E. 'Environmental significance of bedrock jointing in Southern Ontario, Canada'. Environmental Geology, vol. 26, pp: 269–77, 1995.
2. Eyles, N., Arnaud, E., Scheidegger, A. E., and Eyles, C. H. 'Bedrock jointing and geomorphology in southwestern Ontario, Canada: an example of tectonic predesign'. Geomorphology, vol.19, pp: 17–34, 1997.
3. Anselin, L. 'Local indicators of spatial association—LISA'. Geographical Analysis, vol. 27, issue no. 2. Pp: 93-115, 1995.
4. Chen, Y. C., Sung, Q., and Cheng, K. Y. (2003) 'Along-Strike Variations of Morphotectonics Features in the Western Foothills of Taiwan: Tectonic Implications Based on Stream-Gradient and Hypsometric Analysis' Geomorphology, vol. 56, issue no. 1-2, pp: 109-137, 2003.
5. Twidale, C. R. & Campbell, E. M. Australian Landforms: Understanding a Low, Flat, Arid and Old Landscape. Kenthurst, New South Wales: Rosenberg Publishing, 2005.
6. Diniz-Filho, J. A. F., Bini, L. M., and Hawkins, B. A. 'Spatial Autocorrelationand Red Herrings in Geographical Ecology'. Global Ecology and Biogeography,vol. 12, issue no. 1, pp: 53–64, 2003.
7. Gaetani, M., Angiolini, L., Garzanti, E., Jadoul, F., Leven E. Y., Nicora A. &Sciunnach, D. 'Permain stratigraphy in the Northern Karakorum, Pakistan. 'Riv. Ital. Pal. Strat., vol. 101, issue no. 2, pp: 107-152, 1995.

8. Furbish, D.J., & Andrew, J.T. 'The use of hypsometry to indicate long-term stability and response of valley glaciers to changes in mass transfer'. Journal of Glaciology, vol. 30, issue no. 105, 1984.
9. Hurtrez, J. &Lucazeau, F. 'Lithological Control on Relief and Hypsometryin the Herault Drainage Basin (France)'. ComptesRendus de l'Académie des Sciences—Series IIA—Earth and Planetary Science, vol. 328, issue no. 10, pp: 687–694, 1999.
10. Hurtrez, J. E., Sol, C., &Lucazeau, F. 'Effect of Drainage Area on Hypsometry from an Analysis of Small-Scale Drainage Basins in the Siwalik Hills, Central Nepal'. Earth Surface Processes and Landforms, vol. 24, issue no. 9, pp: 799–808, 1999.
11. Hussain, S.H., & Awan, A.A. 'Causative Mechanisms of Terrain Movement in Hunza Valley', report power point slides, viewed 30 August 2014, 2009.
12. Jan, M.Q., &Kazmi, A.H. 'Plate tectonics configuration of Gemstones of Pakistan'. Islamabad: Quaid-i-Azam University, 2005.
13. Keller, E. A., & Pinter, N. Active Tectonics: Earthquakes, Uplift, and Landscape. New Jersey, Prentice Hall, 2002.
14. Kent, R. (1991) 'Lithospheric uplift in easternGondwana: evidence for a long-lived mantle plume sys-tem?'. Geology, vol.19, pp:19–23, 1991.
15. Lifton, N.A. & Chase, C.G. 'Tectonic, climatic and lithological influences on landscape fractal dimension and hypsometry: implications for landscape evolution in the San Gabriel Mountains, California'. Geomorphology, vol. 5, no. 1–2, pp: 77–114, 1992.
16. Mahmood, S.A., &Gloaguen, R. 'Analyzing Spatial Autocorrelation for Hypsometric Integral to Discriminate Neotectonics and Lithologies Using DEMs and GIS'. GIScience and Remote Sensing: John R. Jensen, vol. 48, issue no. 4, 2011.
17. Mayer, L., Introduction to Quantitative Geomorphology: An Exercise Manual.Englewood Cliffs, NJ, Prentice Hall, 1990.
18. Moran, P. A. P. 'Notes on Continuous Stochastic Phenomena'. Biometrika, vol. 37. no. 1–2, pp. 173, 1950
19. Pike, R. J., & Wilson, S. E. 'Elevation-Relief Ratio, Hypsometric Integral,and Geomorphic Area-Altitude Analysis'. Geological Society of America Bulletin,vol. 82, no. 4, pp: 1079–1084, 1971.
20. Pudset, C.J., Schroider, R., Skelton, P.W., &Gupta,V.J., Cretaceous (Aptian/Albian) age for island arc volcanics. Kohistan, N. Pakistan (Contribution to the Himalayan Geology). India, Hindustan Publishing Corporation, 1985.
21. Ratcliffe, J. H., &McCullagh, M. J. 'Identifying Repeat Victimization withGIS'. British Journal of Criminology, vol. 38, issue no. 4, pp: 651–662, 1998.
22. Roohi, R., Dr., Ashraf,A.,Dr., Mustafa, N.,& Mustafa, T. Community Based Survey for Assessment of Glacial Lake Outburst Flood Hazards (GLOFs) in Hunza River Basin. Water Resources Research Institute, National Agricultural Research Centre: Islamabad, 2008.
23. Scheidegger, A. E. 'Morphotectonics of eastern Nepal'. Indian Journal of Landscape Systems andEcological Studies, vol. 22, pp: 1–9, 1999.